

## Electronic Supplementary Information (ESI)

### Molecularly engineered linear organic carbonates as practically viable nonflammable electrolytes for safe Li-ion batteries

Jina Lee,<sup>†ab</sup> A-Re Jeon,<sup>†ab</sup> Hye Jin Lee,<sup>c</sup> Ukseon Shin,<sup>de</sup> Yiseul Yoo,<sup>af</sup> Hee-Dae Lim,<sup>a</sup>  
Cheolhee Han,<sup>h</sup> Hochun Lee,<sup>h</sup> Yong Jin Kim,<sup>c</sup> Jayeon Baek,<sup>\*c</sup> Dong-Hwa Seo,<sup>\*dg</sup> Minah Lee<sup>\*a</sup>

<sup>a</sup> Energy Storage Research Center, Korea Institute of Science and Technology (KIST), 14 Gil 5 Hwarang-ro, Seongbuk-gu, Seoul 02792, Republic of Korea

<sup>b</sup> Department of Chemical and Biological Engineering, Korea University, 02841 Seoul, Korea

<sup>c</sup> Green and Sustainable Materials R&D Department, Korea Institute of Industrial Technology, 89 Yangdaegiro-gil, Ipjang-myeon, Seobuk-gu, Cheonan-si, Chungcheongnam-do, 31056, Republic of Korea

<sup>d</sup> School of Energy and Chemical Engineering, Ulsan National Institute of Science and Technology (UNIST), Ulsan 44919, Republic of Korea

<sup>e</sup> School of Energy and Chemical Engineering, Ulsan National Institute of Science and Technology (UNIST), Ulsan 44919, Republic of Korea

<sup>f</sup> Department of Materials Science and Engineering, Korea University, 145, Anam-ro, Seongbuk-gu, Seoul 02841, Republic of Korea

<sup>g</sup> Department of Materials Science and Engineering, Korea Advanced Institute of Science and Technology (KAIST), Daejeon 34141, Republic of Korea

<sup>h</sup> Department of Energy Science and Engineering, DGIST, Daegu 42988, Republic of Korea

\* E-mail: jbaek@kitech.re.kr (J.B.), dseo@unist.ac.kr (D.-H.S.), minahlee@kist.re.kr (M. L.)

## Experimental details

### Chemicals

Dimethyl carbonate (DMC, 99%), diethyl carbonate (DEC, 99%), 2-methoxyethanol (MEG, 99%), magnesium oxide (MgO, >99%), benzoic acid (99%), and chloroform-d (99.8%, Isotope, contains 0.03% v/v TMS) were purchased from Alfa Aesar. Dibutyl carbonate (DBC, >98%) was purchased from Tokyo Chemical Industry Co., Ltd. Ethylene carbonate (EC, 99%) was obtained from Sigma-aldrich. All of the materials and reagents were used directly without further purification. Fluoroethylene carbonate (FEC,  $\geq 99\%$ ) was provided from Fluorine Korea Co., Korea.

### Bis(2-methoxyethyl) carbonate (BMEC) synthesis

The transesterification reaction was conducted in a 1 L three-necked round-bottomed flask equipped with a dean-stark apparatus and heating mantle. DMC (1 mol), MEG (4 mol), and MgO (15 g) were charged into the reactor, and the temperature was gradually raised to 120°C and kept for 6 h. Then the setting temperature was increased to 130, 140, 150°C every 2 h and kept at 150°C for 2 h. During the reaction, the by-product methanol was removed by the dean-stark apparatus. After the transesterification, vacuum distillation of the crude product was carried out in a 1 L three-necked round-bottomed flask equipped with a distillation column and vacuum pump at 200°C under the pressure of 5 mbar. The purified BMEC was stirred with activated carbon at room temperature overnight. Finally, we obtained clear BMEC after the filtration of activated carbon. The purity of isolated BMEC was analyzed by qNMR with benzoic acid (99%) as an internal standard and the yield of BMEC was calculated based on the mole of isolated BMEC (mmol) per mole of charged DMC (mmol).

### Electrolyte and electrode preparation

All electrolytes were prepared by dissolving 1 M LiPF<sub>6</sub> salt and 3 vol % FEC additive in carbonate solvents. As a conventional electrolyte, 1 M LiPF<sub>6</sub> dissolved in EC/DEC (1:1 vol %) with 3 vol % FEC was used for comparison.

To test the compatibility of the tailored electrolyte with conventional electrodes materials, we used LiNi<sub>0.83</sub>Co<sub>0.11</sub>Mn<sub>0.06</sub>O<sub>2</sub> (NMC811, COSMO AM&T CO., Korea) and graphite (Hitachi, Japan) as cathode and anode material examples in half-cell tests. The NMC811 electrode was prepared by mixing NMC811, super P, and polyvinylidene fluoride (Solvay, Belgium) binder in a 90:5:5 weight ratio using N-methyl-2-pyrrolidone (NMP) solvent. The graphite electrode was prepared by mixing graphite, super P, and aqueous binder (Aekyung chemical Co., Korea) in an 85:5:10 weight ratio using water. The slurries were mixed using a planetary centrifugal mixer (ARE-310, THINKY, USA) and casted on aluminum (for cathode) or copper foil (for anode), followed by vacuum drying at 80°C overnight. The thickness of the NMC811 electrode was 25  $\mu\text{m}$  after calendaring and the active mass loading was  $\sim 3.5 \text{ mg cm}^{-2}$ . The thickness of the graphite electrode was 40  $\mu\text{m}$  after calendaring and the active mass loading was  $\sim 1.5 \text{ mg cm}^{-2}$ .

### Electrochemical tests

Ionic conductivities of electrolytes were measured using ion-blocking symmetric cells with stainless steel electrodes (SS) in CR2032 coin cells. 70  $\mu\text{L}$  of electrolytes were used for glass fiber separators (Whatman, GF/F). The EIS measurement of the SS||SS cells was conducted over a frequency range of 1 MHz to 300 mHz in a temperature range from 0 to 45°C using ZIVE SP1 (WonATech Co. Ltd., South Korea). The ionic conductivity ( $\sigma$ ) was calculated by using an equation,  $\sigma = L R^{-1} A^{-1}$ , where L is the distance between two SS electrodes, A is the area of the electrodes, and R is the resistance measured by EIS.

The lithium transference number ( $t_{\text{Li}^+}$ ) of electrolytes was estimated by a combination of AC impedance and DC polarization techniques using Li||Li symmetric cells with GF/F separators. Li metal chips (11.3 mm, 450  $\mu\text{m}$ ) were used as the electrode. The step potential amplitude was 10 mV. The  $t_{\text{Li}^+}$  was

calculated using the Bruce–Vincent equation.<sup>1</sup> The measurement was conducted by VMP3 potentio/galvanostat (Bio-logic Scientific Instruments, France) at 30°C.

*The anodic stability of the electrolyte* was tested by galvanostatic cycling of the Li||Li symmetric cells using GF/F and Celgard 2320 separators. The cells were cycled at a current density of 1 mA cm<sup>-2</sup> for 0.5 h with voltage cut off of 1 V. The electrolyte/capacity ratio was 140  $\mu$ l mAh<sup>-1</sup>.

*The Li||Cu cell test* was carried out with asymmetric cells (Li||Cu) using a Li metal chip (11.3 mm), Copper foil (16 mm), and a GF/F separator. The Li||Cu cells were cycled within a voltage range of -1 to 1 V at a current density of 1.0 mA cm<sup>-2</sup> and areal capacity of 0.5 mAh cm<sup>-2</sup>.

*The LSV test* was conducted with Li||Al asymmetric cells using a GF/F separator. The Li||Al cells were initially cycled for 3 times between OCV to 3.5 V to alleviate the overpotential from Li metal anode at a scan rate of 5 mV s<sup>-1</sup> and then charged from OCV to 5.5 V at a scan rate of 1 mV s<sup>-1</sup>.

*The CV test* was performed to confirm the oxidation stability of electrolytes. The Li||Al asymmetric cells with a GF/F separator were cycled in a voltage range of 2.7–4.3 V at a scan rate of 1 mV s<sup>-1</sup>.

*Half-cell tests* were conducted using a WBCS-3000 battery cycler (Wonatech Co. Ltd., Korea) with CR2032 coin cells. The cell casing (bottom, top, gasket, spacer (0.8t) and spring) was 3.25 g, and GF/F was 15 mg. The electrolyte/capacity ratio of Li||NMC811 and Li||graphite half cells was 95  $\mu$ l mAh<sup>-1</sup> and 120  $\mu$ l mAh<sup>-1</sup>, respectively. The *NMC811 half cells* were cycled at a current density of 0.1C for 3 cycles and then at 0.5C. (1C = 200 mAh g<sup>-1</sup>) in a voltage range of 2.7–4.3 V. The coulombic efficiencies of E1D1, BMEC and B7E3 cells in the 3rd cycle were 99.8%, 99.5% and 99.3%, respectively. The rate capability was tested by gradually increasing the C-rate (1C = 200 mAh g<sup>-1</sup>) from 0.5C to 4C after two formation cycles at 0.1C. *The graphite half cells* were cycled at 0.2C for 2 cycles and then at 0.5C (1C = 372 mAh g<sup>-1</sup>) in a voltage range of 0.03–1.2 V. After galvanostatic discharge, a constant voltage (CV) step was applied until the current density decreased to 0.02C. The coulombic efficiencies of E1D1, BMEC and B7E3 cells in the 200th cycle were 98.7%, 98.8% and 98.4%, respectively.

### **Pouch cells for long-term cycling and nail-penetration tests**

1-Ah and 4-Ah graphite||NMC811 pouch cells were prepared by Wellcos Co., Korea using lab-made B7E3 and E1D1 electrolytes and polyethylene separator (CangZhou MingZhu Plastic Co. Ltd., China). The sizes of cathode (94 wt % NMC811) and anode (96 wt % graphite) sheets were 47.0 and 49.8 cm<sup>2</sup>, respectively. In the 1-Ah graphite||NMC811 pouch cells, the mass loading of the cathode and anode was 35.6 mg cm<sup>-2</sup> and 22.0 mg cm<sup>-2</sup> per sheet, respectively. In the 4-Ah graphite||NMC811 pouch cells, the mass loading of the cathode and anode was 42.0 mg cm<sup>-2</sup> and 22.4 mg cm<sup>-2</sup> per sheet, respectively. To test the long-term stability of the tailored electrolyte, the 1-Ah graphite||NMC811 pouch cell was cycled at a current density of 0.1C for 2 cycles and then at 0.3C within a voltage range between 2.75 V to 4.2 V. The average charge and discharge voltages of the BMEC cells at 0.1C were 3.78 V and 3.69 V, respectively. For E1D1, the average charge and discharge voltages were 3.77 V and 3.65 V, respectively. The 4-Ah pouch cells were used in the nail-penetration test. Before the penetration, the 4-Ah pouch cells were cycled at 0.1C for 2 cycles within a voltage range between of 2.75 V to 4.2 V and then charged to 3.9 V. At 3.9 V, the capacities of the E1D1 and BMEC cell were 2.61 and 2.65 Ah, respectively.

### **Characterization techniques**

*The viscosity of electrolytes* was measured using a rheometer (DHR-3, TA instrument, USA) at 25°C.

*Near-edge X-ray absorption fine-structure spectroscopy (NEXAFS)* was conducted to analyze the SEI composition of the cycled graphite anode. The NEXAFS experiment was performed at the X-ray 10D XAS KIST beamline in the Pohang Accelerator Laboratory (PAL, Pohang, Korea). Sampling was carried out under an argon atmosphere in a glove box. The sample holder was sealed with an aluminum pouch to prevent air exposure and immediately transferred to the vacuum chamber of the NEXAFS equipment.

*Fourier transform infrared spectroscopy (FTIR)* was conducted to compare the degree of C=O participation in solvating Li ions and degree of salt dissociation in each solvent system. The FTIR

spectra were obtained using an AlphaII (Bruker, USA) spectrometer under an argon atmosphere.

*<sup>7</sup>Li Nuclear magnetic resonance (NMR) measurements* were performed on a 600 MHz Agilent instrument. External standards containing 1 M LiCl in D<sub>2</sub>O were inserted into each sample in the form of a coaxial-sealed capillary.

*High-resolution transmission electron microscopy (HR-TEM) analysis* was carried out to investigate the surface of NMC811 cathode. The cathodes were obtained from NMC811 half cells after being fully charged to 4.3 V. The half cells were disassembled in an argon-filled glovebox and the retrieved NMC cathodes were rinsed with pure DMC. After drying under vacuum, the cathode powder was gently scrapped from the aluminum current collector and dispersed in DMC. The dispersion solution was dropped on a Copper TEM grid (200 mesh, Sigma-aldrich) and dried for 5 minutes. The as-prepared samples were analyzed using a TEM (TITANTM 80-300, Thermofisher, US) operated at 300 kV. The available point resolution is better than 1 Å at an operating accelerating voltage. Images were recorded by a 4k × 4k CCD (Oneview 1095, Gatan, US) camera.

*X-ray diffraction (XRD) analysis* was performed with XRD diffractometer (Miniflex2, Rigaku, Japan) with Cu K-alpha beam source. The charged NMC811 cathode before and after heating at 235°C for 15 min were sealed with Kapton tape inside an argon-filled glovebox.

### **Thermal stability analyses**

*The boiling point of electrolytes* was determined by OECD Test Guideline 103, distillation method using distillation apparatus. The liquid sample was distilled, and the vapor recondensation temperature was measured when the temperature maintained for 4 min. The maintained vapor recondensation temperature is the boiling point.

*The flash point of electrolytes* was determined by KS M ISO 3679 method using OptiFlash Small Scale (PAC, USA). The liquid sample was slowly charged into the cell by syringe, and the amount of sample depended on the flash point (when the flash point is lower than 100°C: 2 mL; when the flash point is over 100°C: 4 mL). The sample was stabilized for 1 min; then, applied the ignition to find the flash point every 5°C, which was repeated until the sample was ignited. After roughly identifying the flash point, a fresh sample was tested every 2°C and then every 0.5°C to get the accurate flash point.

*The self-extinguishing time (SET)* was carried out in a convection oven at 50°C. For The temperature and humidity for the test were measured by a thermo-humidity meter (Testo 605i). A given mass of solvents (between 0.3 to 0.35 g) was placed on a stainless-steel dish and exposed to a gas burner (K1, Needco, Korea) for 3 s to allow ignition. The ignition time was increased up to 10 s for the solvents that could not be ignited within 3 s, and the flame exposure was repeated more than 3 times. The SET was normalized by the mass of the solvent (s g<sup>-1</sup>). Each solvent was measured 5 times, and the average value was used as a SET value.

*Differential scanning calorimetry (Q2000, TA instrument, USA)* was conducted to investigate thermal reactions between the charged cathodes and electrolytes. The cathode was retrieved from NMC811 and NMC622 half cells after being fully-charged to 4.3 V. The retrieved NMC cathode was vacuum-dried after washing with pure DMC, then the cathode powder was separated from the aluminum current collector. A fresh electrolyte and the retrieved cathode powder (5:2 weight ratio) were sealed in a Tzero aluminum hermetic pan and then heated from 50 to 400°C at the heating rate of 5°C under the nitrogen gas flow rate of 30 ml min<sup>-1</sup>.

*Gas analysis* was conducted with a mass spectrometer (HPR-20 R&D, Hiden Analytical) to analyze the amount and composition of reactive gas generated from electrolyte/cathode mixtures upon external heating. The fully-charged cathode was retrieved from NMC811 half cells at 4.3 V after three formation cycles at 0.1C. A fresh electrolyte and the charged cathode powder (in a 4:1 weight ratio) were sealed in a vial with an aluminum seal and then heated at 235°C for 25 min. After cooling down the sample to room temperature, the evolved gas in the sealed vial was injected into a mass spectrometer using a needle through the septa of the cap. The gas analysis was also performed in the same way for samples containing 40 µl electrolytes without cathode.

*Nail-penetration test* to simulate an internal short circuit was conducted according to the standard SAE J2464 under open air at room temperature using a nail penetration test system installed at RTL Co., Korea. A 4-Ah pouch cell charged to 3.9 V was fixed to a custom-made jig and connected to a potentiostat to monitor the voltage drop during the penetration. The temperature of the shorted battery was monitored with both temperature sensors attached to the pouch surface and a thermal imaging camera. A steel nail with a diameter of 3 mm was moving at a speed of 80 mm s<sup>-1</sup> to vertically penetrate through the cell. We also record the experiment with a smartphone camera.

*Accelerating Rate Calorimeter (ARC) tests* (BTC-130, HEL, England) were conducted to investigate the thermal stability of 1-Ah scale graphite||NMC811 pouch cells. Prior to the ARC tests, the pouch cells were charged up to 4.2 V under constant current conditions at a 0.2C-rate. The cells attached with K-type thermocouple by insulation Kapton tape were placed in the ARC chamber, then a typical Heat-wait-search (HWS) test was conducted. The start temperature was 50°C with a temperature increase of 5°C per each step. The exothermic limit was set to 0.02°C min<sup>-1</sup>, for searching self-heating of the cells. Once self-heating was detected, ARC tracked the change of temperature until the thermal runaway happens. The terminal temperature was set to 350°C, for ensuring the ARC go into the cooling mode.

### Calculation techniques

*Classical molecular dynamics (cMD) simulations* were performed using the Materials Studio software package. The parameters for the Lennard-Jones interaction and the Coulombic interaction refer to the value in the COMPASS III force field<sup>2,3</sup>. Calculations of the Lennard-Jones interaction were performed using the Ewald summation and the cutoff distance was set at 12 Å. The particle-particle-particle-mesh (PPPM) method was used for long-range Coulombic interactions. The amorphous cell module of Materials Studio software was used to build the model (simulation box) for cMD simulations. The number of particles contained in the simulation box was set to each electrolyte that had a 1 M molar concentration, and the optimal combinations to have the same molar concentration was calculated. Two simulation box sizes were considered. The "small-sized" box contained 140 solvent molecules and 23, 27, and 17 LiPF<sub>6</sub> for BMEC, DBC, and DEC, respectively. The "large-sized" box contained 248 solvent molecules and 41, 48, and 30 LiPF<sub>6</sub> for BMEC, DBC, and DEC, respectively. The parameters used for the calculations were the same regardless of the box size. The pressure was set to 1.013e<sup>-5</sup> GPa and the temperature to 298K.

*The geometry optimization function in the Forcite module of Materials Studio software* was used for geometric optimization. This process used a Smart algorithm, which is a cascade of the Steepest Descent, ABNR, and Quasi-Newton methods. The convergence tolerance used was 0.001 kcal mol<sup>-1</sup> for Energy and 0.5 kcal mol<sup>-1</sup> Å for Force.

*NPT simulations* were performed using the Dynamics functions of the same module. Calculation of NPT dynamics is used to relax the model before observing particle motion, and density is optimized in this process. The same temperature and pressure conditions were used in the model building. We used 1.0 fs for the time step and set the total simulation time to 500 ps. Total simulation times were determined based on the observation that regardless of the initial configuration, they converge to a constant density value. We used NHL for the thermostat and 0.01 for the Q ratio. Berendsen was used for the barostat, and 0.1 ps was used as Decay constant. NPT simulation results confirmed that the calculated and measured densities exhibit an error rate of less than 0.3% (Table S4).

*NVT simulations* were performed using the same functions used in NPT simulations. The motion of the particles was observed using NVT dynamics calculations. Time step, temperature, and thermostat are the same as NPT simulation values. The total simulation time was 3 ns to obtain accurate MSD.

*Mean squared displacement (MSD) analysis* was performed to understand the degree of diffusion of lithium ions. The analysis target was lithium ion, and all 3 ns NVT trajectories were used for the analysis,

but the early 10% and the latter 10% intervals showing nonlinearity were excluded in order to accurately grasp the degree of diffusion. The diffusivity was calculated by  $\lim_{t \rightarrow \infty} \frac{MSD}{6t}$ .

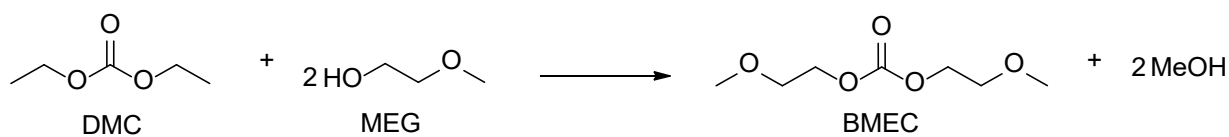
*Density functional theory (DFT) method* was used for all quantum mechanical calculations with Becke's three parameters (B3) exchange functional in Lee-Yang-Parr (LYP) nonlocal correlational functional (B3LYP).<sup>4</sup> Geometry optimization and energy calculations were performed at the B3LYP/6-31++G(d,p) level. All calculations including highest occupied molecular orbital (HOMO)/lowest unoccupied molecular orbital (LUMO) calculations and electrostatic potential (ESP) calculations were performed using the Gaussian 16 software package.<sup>5</sup>

*Solvation shell analysis* to grasp the dissociation degree of LiPF<sub>6</sub> for each solvent was performed by trajectory analysis of NVT simulation using Pymatgen library.<sup>6</sup> The trajectory of the NVT simulation was analyzed structurally by exporting to a crystallographic information file (CIF) at intervals of 100 ps, and the CIF structure files were analyzed using the Pymatgen library. The degree of dissociation was grasped by judging dissociation when there was no F atom within the solvation radius of each Li-ion. The solvation radius was set to  $2.03 \pm 0.06$  Å according to Kameda's method,<sup>7</sup> and dissociation analysis was performed on five points of 1.97, 2.00, 2.03, 2.06, and 2.09 Å to identify the overall trend. The degree of dissociation was analyzed for three independent cMD simulations for each solvent, and the graph (Fig. 3g) was presented through mean and standard deviation.

*An analysis to identify the number of oxygen atoms in the solvation shell* was also performed on the same CIF files using the pymatgen library. At this time, the value of 2.08 Å, which is the Li-O interatomic distance reported by Kameda et al.,<sup>7</sup> was used as the radius for determining the solvation shell. The numbers were obtained by averaging after counting the number of O atoms in the radius for each Li ion. (Fig. 3h) To examine the overall trend, we analyzed number of oxygen atoms in solvation shell based on solvation radius from 1.9 to 2.4 Å at 0.1 Å intervals. (Fig. S18)

*Prediction of boiling points using machine learning* was performed using the scikit-learn module<sup>8</sup> in Python. The descriptors used for regression were adopted from a previous QSAR-based study.<sup>9</sup> Among the descriptors presented in the paper, we calculated the Pearson coefficient to find the two variables with the highest correlation to the measured boiling point, which turned out to be polarizability and molecular weight. The molecules used for predicting boiling points were based on (2-methoxyethyl) methyl carbonate (MEMC) for asymmetric carbonate molecules and BMEC for symmetric carbonate molecules, and boiling points were predicted according to the extended length of the alkyl chain.

$$\text{Isolated BMEC yield} = \frac{\text{BMEC produced (mmol)}}{\text{DMC charged (mmol)}} \times 100$$



Product	Isolated yield
 BMEC	43.2%

**Fig. S1** Reaction scheme of transesterification of dimethyl carbonate (DMC) with 2-methoxyethanol (MEG) to form bis(2-methoxyethyl) carbonate (BMEC) and the isolated yield of BMEC.

$$P_{\text{BMEC}} = \frac{I_{\text{BMEC}}}{I_{\text{std}}} \times \frac{N_{\text{std}}}{N_{\text{BMEC}}} \times \frac{M_{\text{BMEC}}}{M_{\text{std}}} \times \frac{W_{\text{std}}}{W_{\text{BMEC}}} \times P_{\text{std}}$$

Where,

$P_{\text{BMEC}}$ : The purity of the isolated BMEC.

$P_{\text{std}}$ : The purity of the standard (benzoic acid, purity = 99%).

$I_{\text{BMEC}}$ : The integrated area of BMEC signal.

$I_{\text{std}}$ : The integrated area of benzoic acid.

$N_{\text{BMEC}}$ : The number of BMEC protons (proton signal of  $\delta$  4.29).

$N_{\text{std}}$ : The number of benzoic acid protons (proton signal of  $\delta$  8.13).

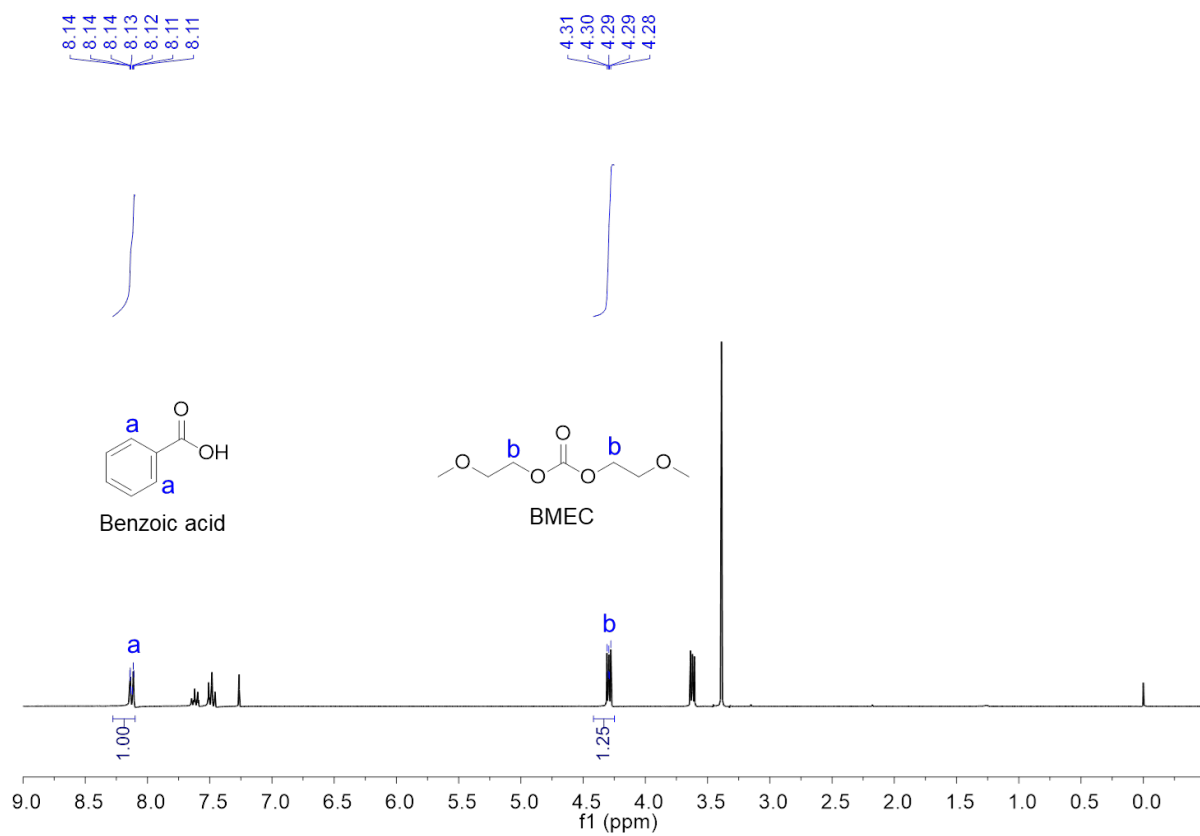
$M_{\text{AA}}$ : The molecular mass of BMEC ( $\text{g mol}^{-1}$ ).

$M_{\text{std}}$ : The molecular mass of benzoic acid ( $\text{g mol}^{-1}$ ).

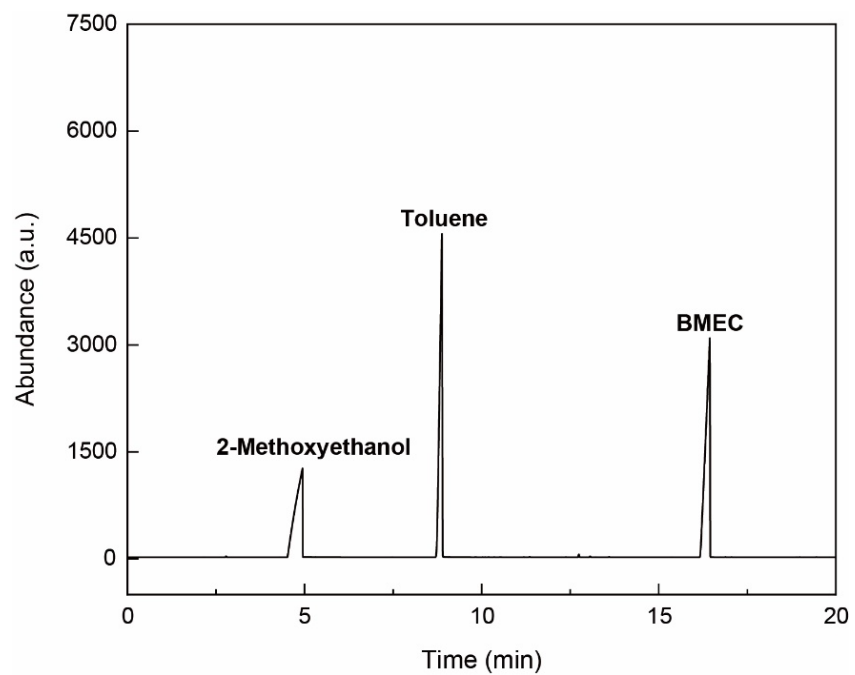
$W_{\text{AA}}$ : The gravimetric weight of BMEC (mg).

$W_{\text{std}}$ : The gravimetric weight of benzoic acid (mg).

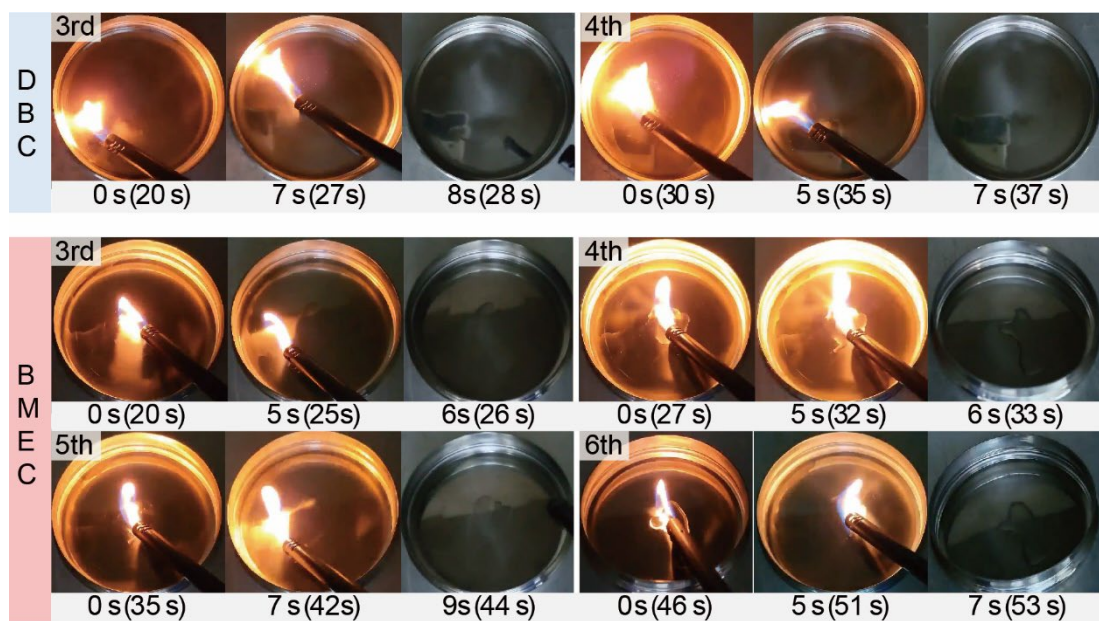
**Fig. S2** Purity of isolated BMEC. The isolated BMEC purity was analyzed using qNMR with absolute concentration determination. Benzoic acid (Alfa Aesar, purity = 99%) was used as an internal standard. About 5 mg of standard and 5 mg of isolated BMEC were added to the NMR tube. Then the mixture was fully dissolved in 0.6 mL of  $\text{CDCl}_3$  to obtain a solution with a concentration of about  $15 \text{ mg mL}^{-1}$ .  $^1\text{H}$  NMR spectra of the samples were obtained on Bruker NMR 300 MHz. The spectra of samples were integrated for calculating the purity of the isolated BMEC (Fig. S3). The purity of BMEC was determined using the following formula.<sup>10</sup>



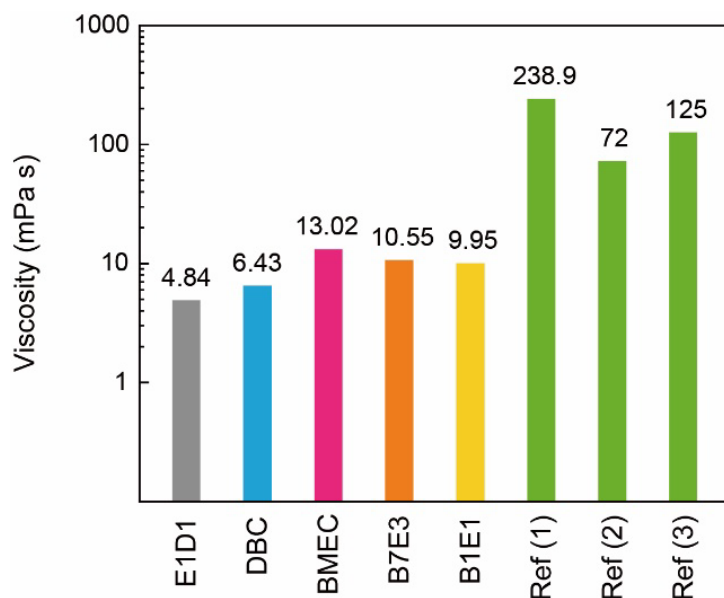
**Fig. S3** Integrated peaks of  $^1\text{H}$  qNMR spectra of isolated BMEC using benzoic acid as an internal standard in  $\text{CDCl}_3$ .  $^1\text{H}$  qNMR : BMEC  $\delta$  4.29 (m, 4H); benzoic acid  $\delta$  8.13 (m, 2H).



**Fig. S4** A gas chromatogram of the product after transesterification of DMC with 2-methoxyethanol, with toluene used as an internal standard.



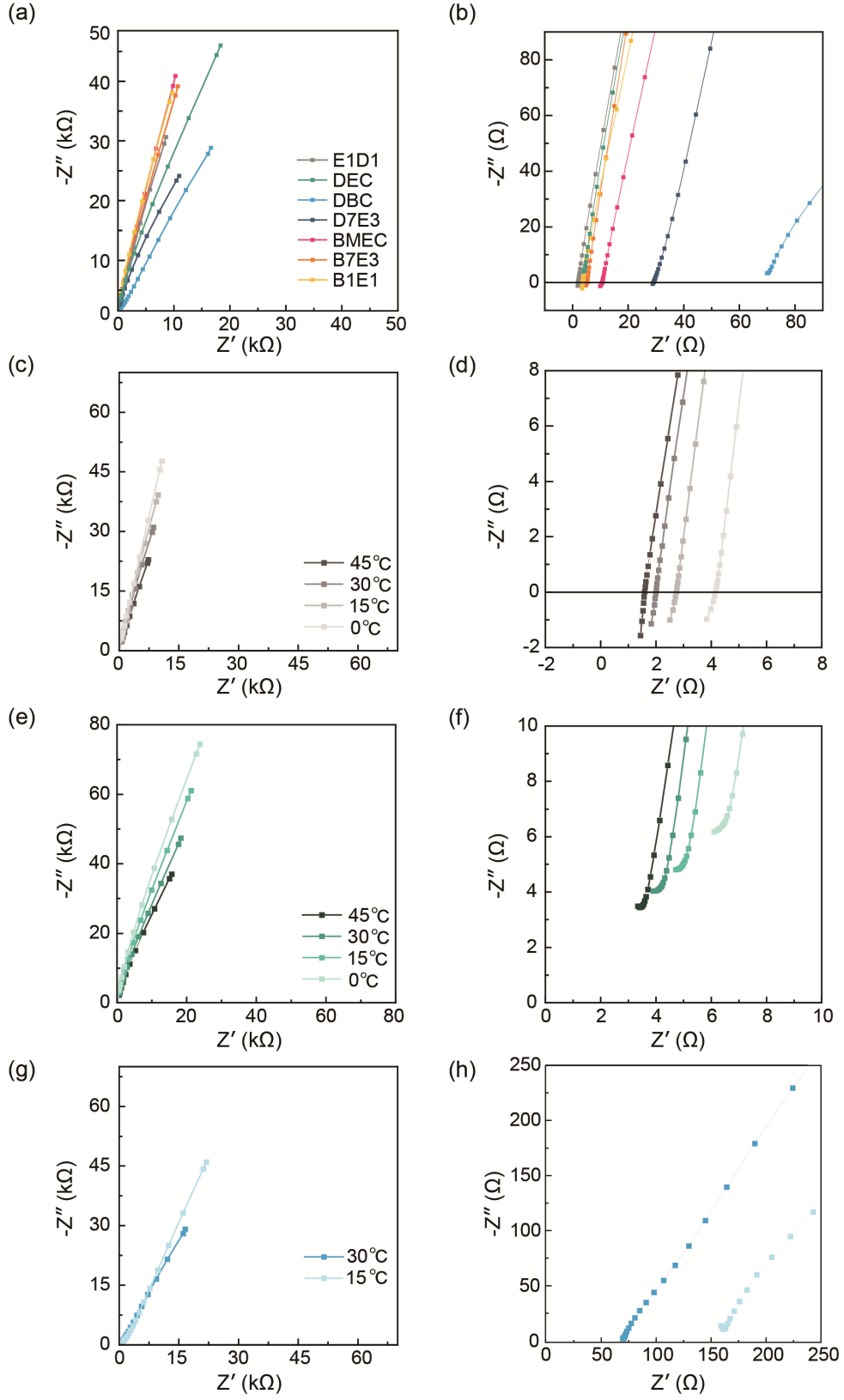
**Fig. S5** Photographs capturing the self-extinguish time (SET) test of solvents at 50°C after second trials of ignition in Fig. 1d. The DBC and BMEC solvents were not ignitable even after 4 and 6 attempts, respectively. The time outside parentheses is the time run on each trial, and the time in parentheses is the run time shown in Video S2 (for DBC) and Video S3 (for BMEC)



**Fig. S6** The viscosities of electrolytes using different solvents at 25°C. Each electrolyte contains 1 M LiPF<sub>6</sub> and 3 vol% FEC additive. The viscosity was measured at a shear rate of 103 s<sup>-1</sup>. We also compared the viscosity values of other nonflammable electrolyte examples including the high concentration electrolyte (HCE) and ionic liquids.

Reference list of the nonflammable electrolyte examples in Fig. S6

1. J. Wang, Y. Yamada, K. Sodeyama, C. H. Chiang, Y. Tateyama and A. Yamada, *Nat. Commun.*, 2016, **7**, 12032.
2. J. Wang, Y. Yamada, K. Sodeyama, E. Watanabe, K. Takada, Y. Tateyama and A. Yamada, *Nat. Energy*, 2017, **3**, 22-29.
3. H. Sun, G. Zhu, Y. Zhu, M. C. Lin, H. Chen, Y. Y. Li, W. H. Hung, B. Zhou, X. Wang, Y. Bai, M. Gu, C. L. Huang, H. C. Tai, X. Xu, M. Angell, J. J. Shyue and H. Dai, *Adv. Mater.*, 2020, **32**, e2001741



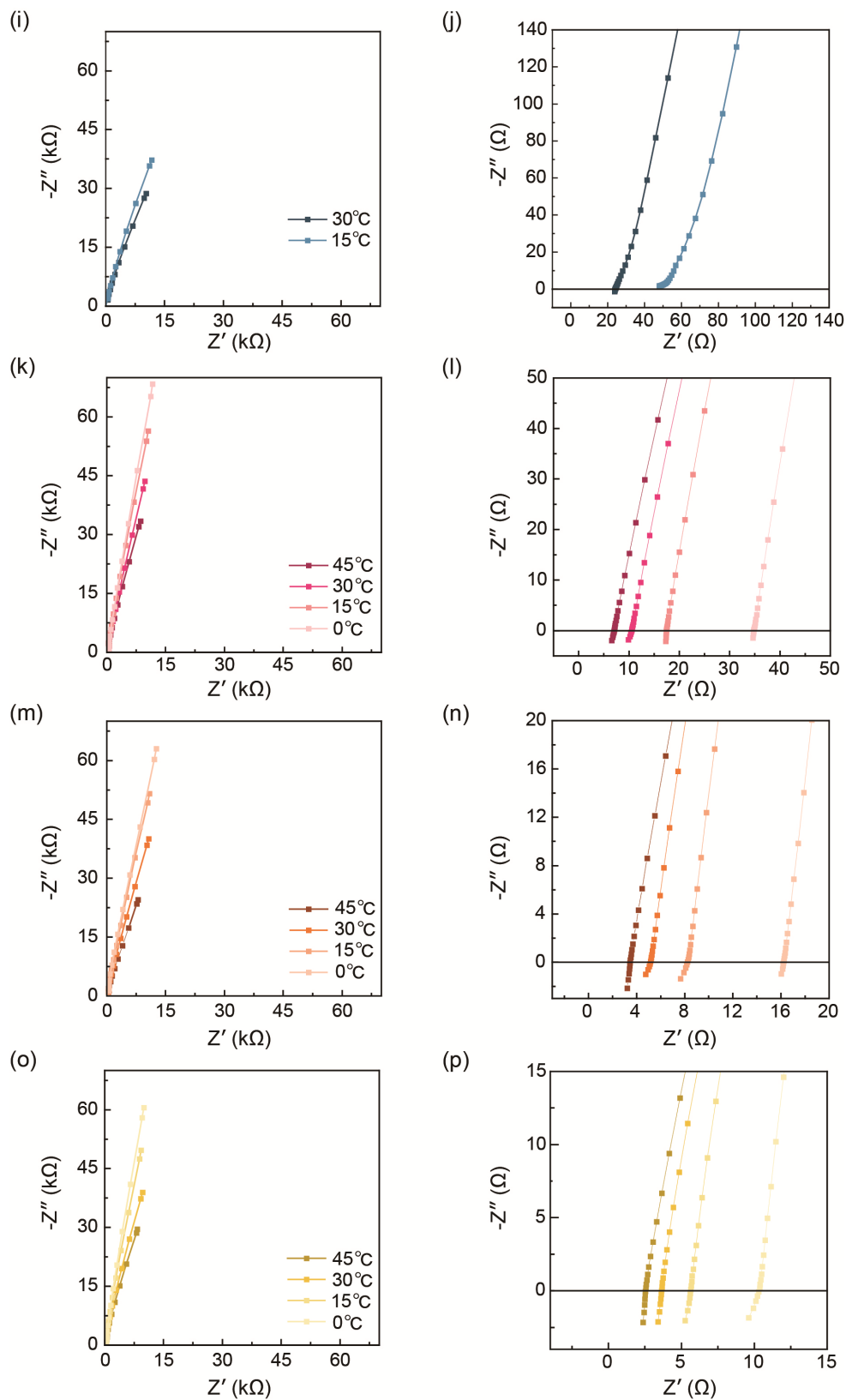


**Fig. S7** (a) Nyquist plots of SS||SS cells in different electrolytes and (b) the corresponding enlarged curves at 30°C. Nyquist plots and their enlarge curves of (c, d) E1D1, (e, f) DEC, (g, h) DBC, (i, j) D7E3, (k, l) BMEC, (m, n) B7E3 and (o, p) B1E1 measured every 15°C over a temperature range from 0°C to 45°C

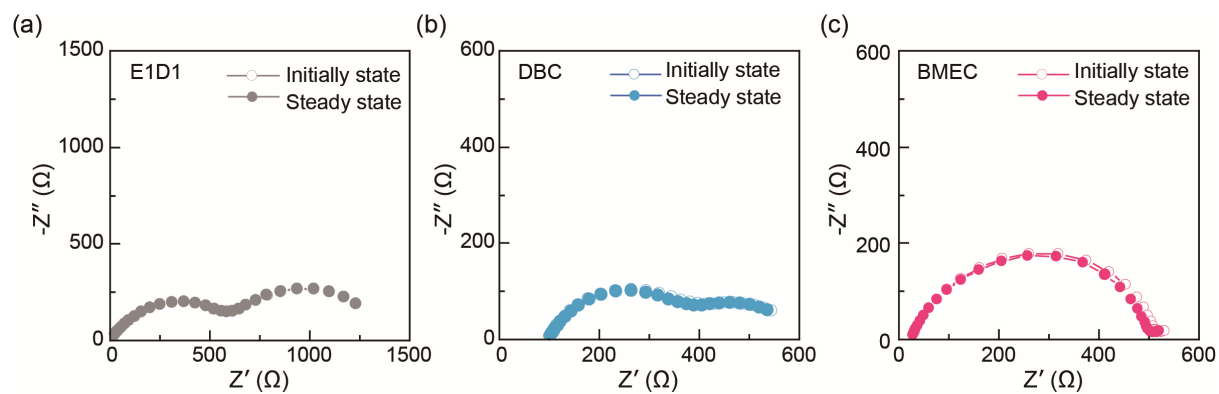


**Fig. S8** Nyquist plots of Li||Li cells using (a) E1D1, (b) DBC, and (c) BMEC electrolytes before and after the DC polarization (Fig. 2b) used for transference number calculation.

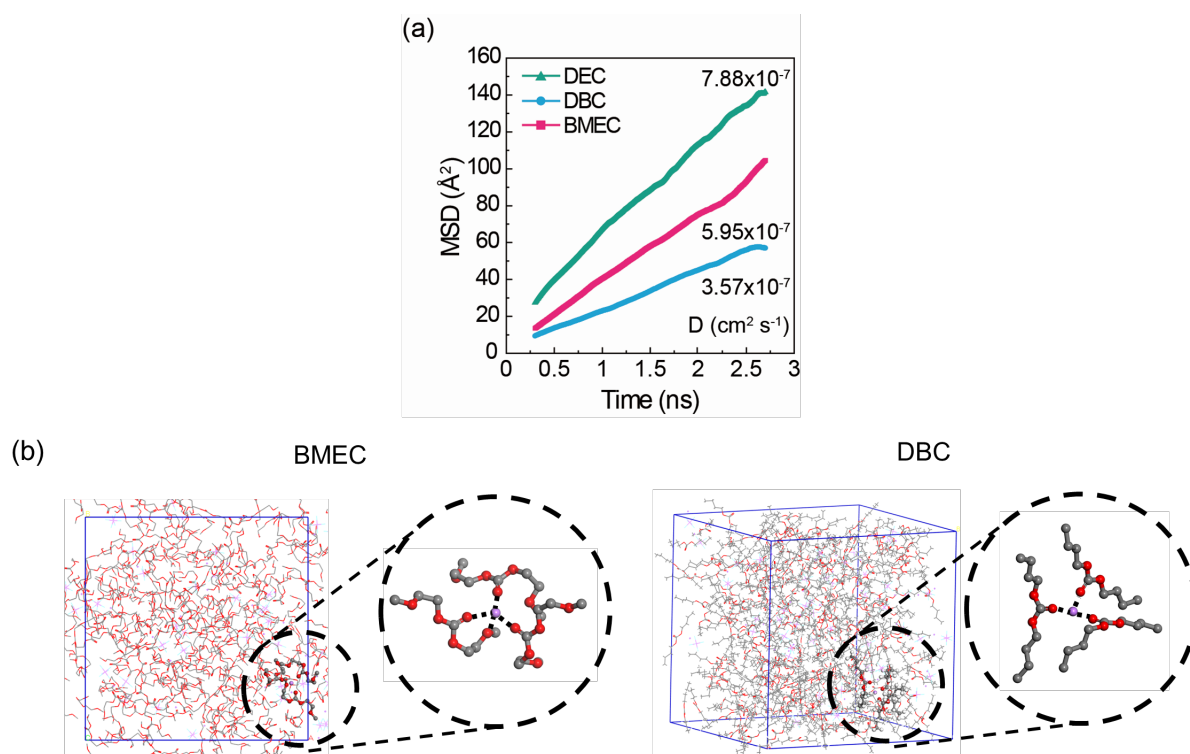


**Fig. S9** (a) Representative mean squared displacement (MSD) results from three independent cMD simulations for each solvent in large-sized boxes containing 248 solvent molecules. (b) Configuration of the simulation system for BMEC and DBC electrolytes.

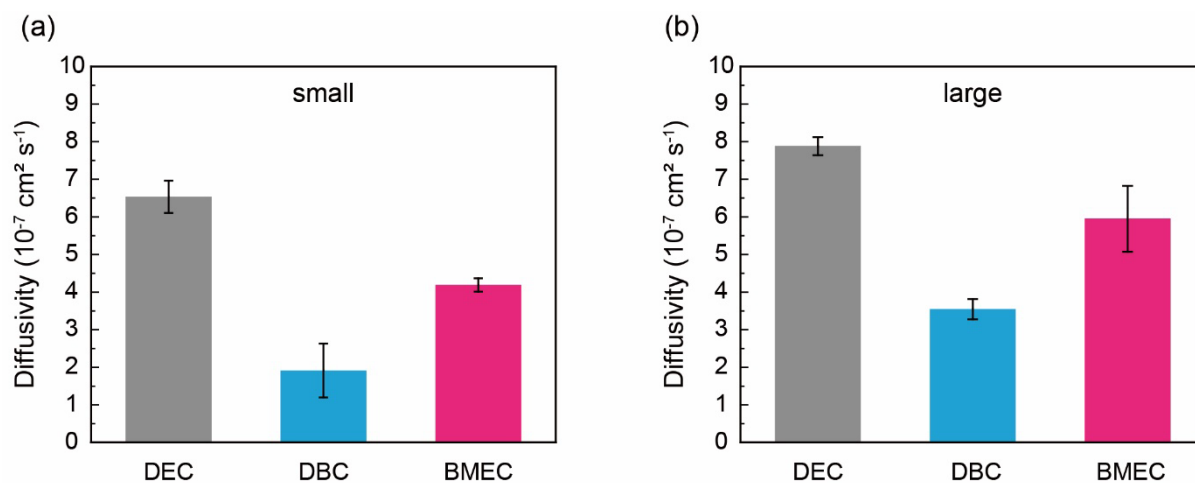


**Fig. S10** Statistical analysis of diffusivity data for all three independent cMD productions. In the graph legend, "small" refers to a system composed of 140 solvent molecules and  $\text{LiPF}_6$  ions of 23, 27, and 17 for BMEC, DBC, and DEC, respectively, while "large" refers to a system composed of 248 solvent molecules and  $\text{LiPF}_6$  ions of 41, 48, and 30 for BMEC, DBC, and DEC, respectively. Regardless of whether it is "small" or "large," it can be confirmed that the order and trends are maintained.

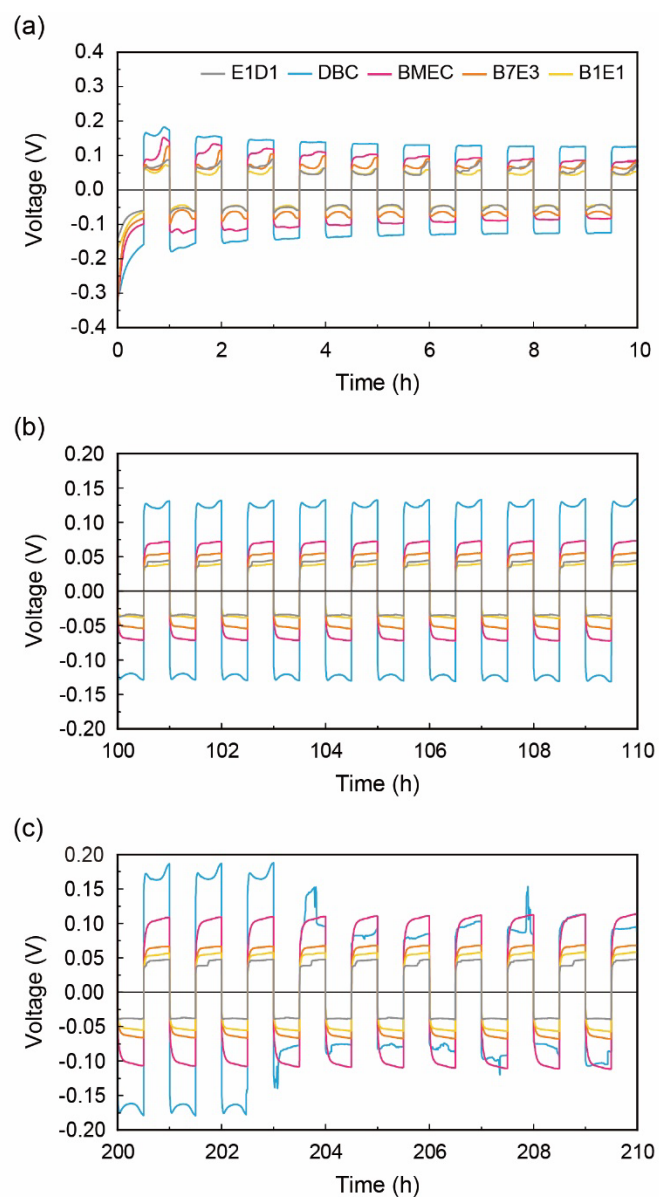


**Fig. S11** Voltage profiles of Li||Li symmetric cells with GF/F separators using different electrolytes in the (a) 1–10th cycles, (b) 100–110th cycles, and (c) 200–210th cycles. The Li||Li symmetric cells were cycled at a current density of  $1.0 \text{ mA cm}^{-2}$  and areal capacity of  $0.5 \text{ mAh cm}^{-2}$ .

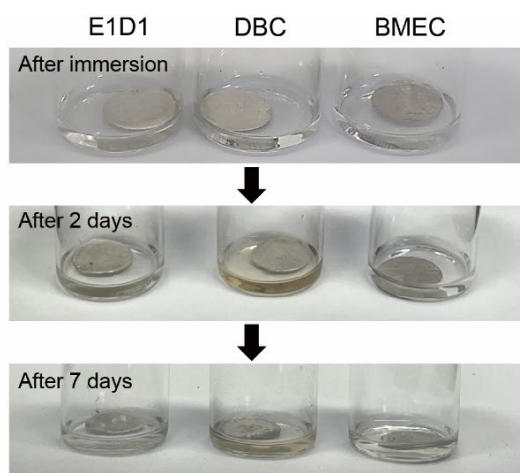


**Fig. S12** Reduction stability of electrolytes on Li metal. The Li metal chip (16 mm diameter) was immersed in 2 ml of each electrolyte, and the color change of the electrolytes was observed. Initially, all electrolytes were transparent after Li metal soaking, but after 2 days, the DBC electrolyte turned yellowish. Even after 7 days, E1D1 and BMEC still remained transparent, indicating their chemical stability versus Li metal.

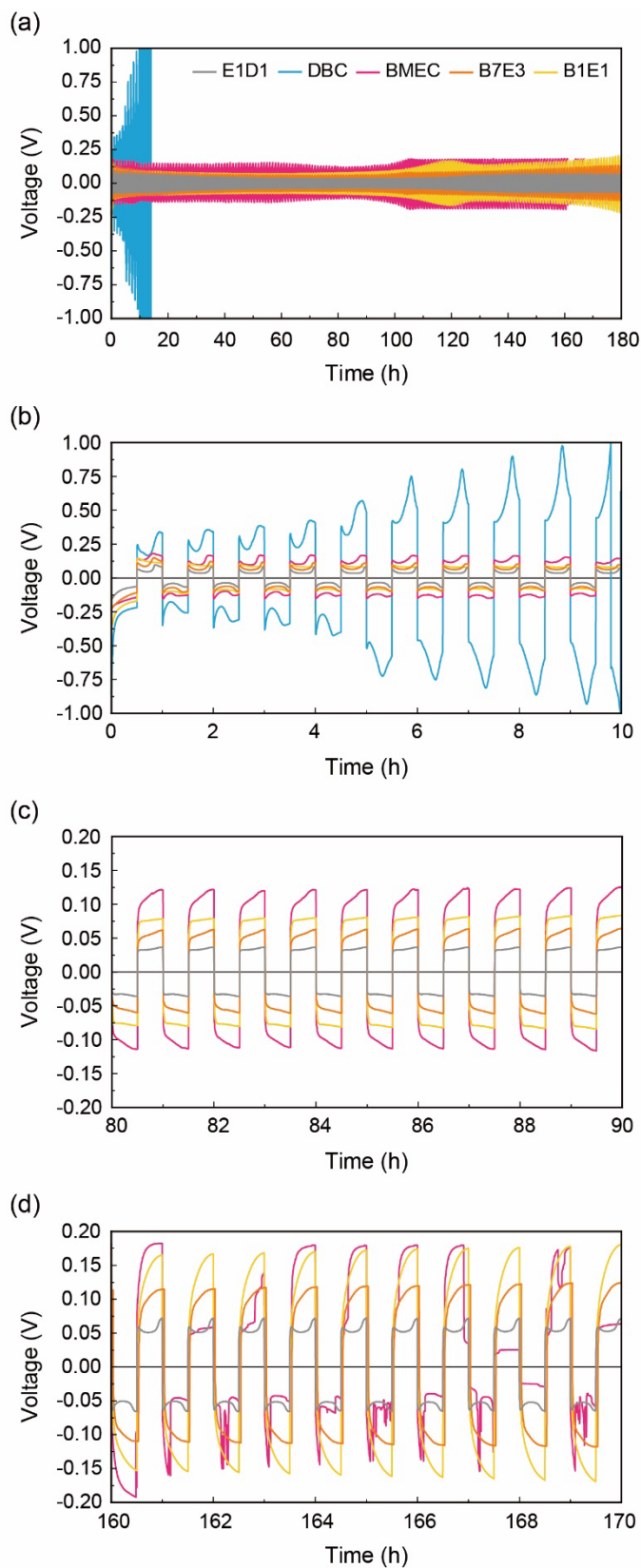


**Fig. S13** (a) Voltage profiles of Li||Li symmetric cells using Celgard 2320 separators in different electrolytes and their enlarged curves in the (b) 1–10th, (c) 80–90th, and (d) 160–170th cycles. Li||Li symmetric cells were cycled at a current density of  $1.0 \text{ mA cm}^{-2}$  and areal capacity of  $0.5 \text{ mAh cm}^{-2}$ .

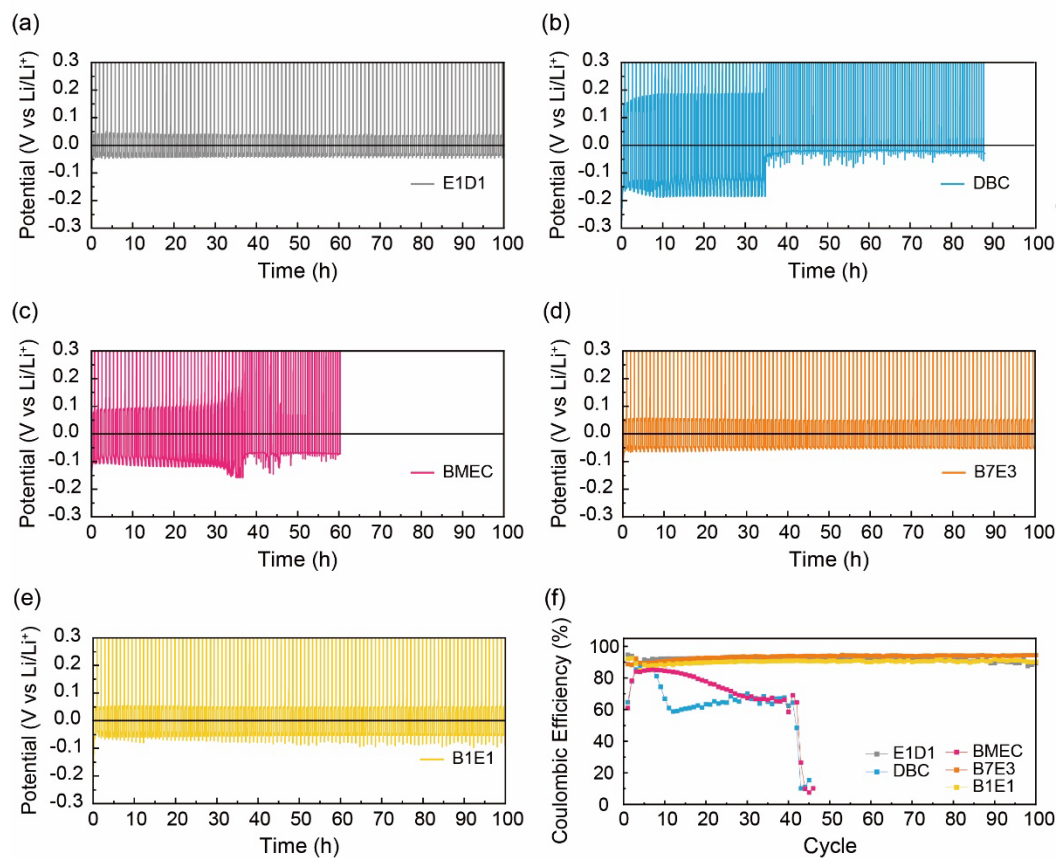


**Fig. S14** Voltage profiles of Li||Cu cells with GF/F separators using (a) E1D1, (b) DBC, (c) BMEC, (d) B7E3, and (e) B1E1. (f) Coulombic efficiencies of Li||Cu cells cycled in different electrolytes at a current density of  $1.0 \text{ mA cm}^{-2}$  and areal capacity of  $0.5 \text{ mAh cm}^{-2}$ .

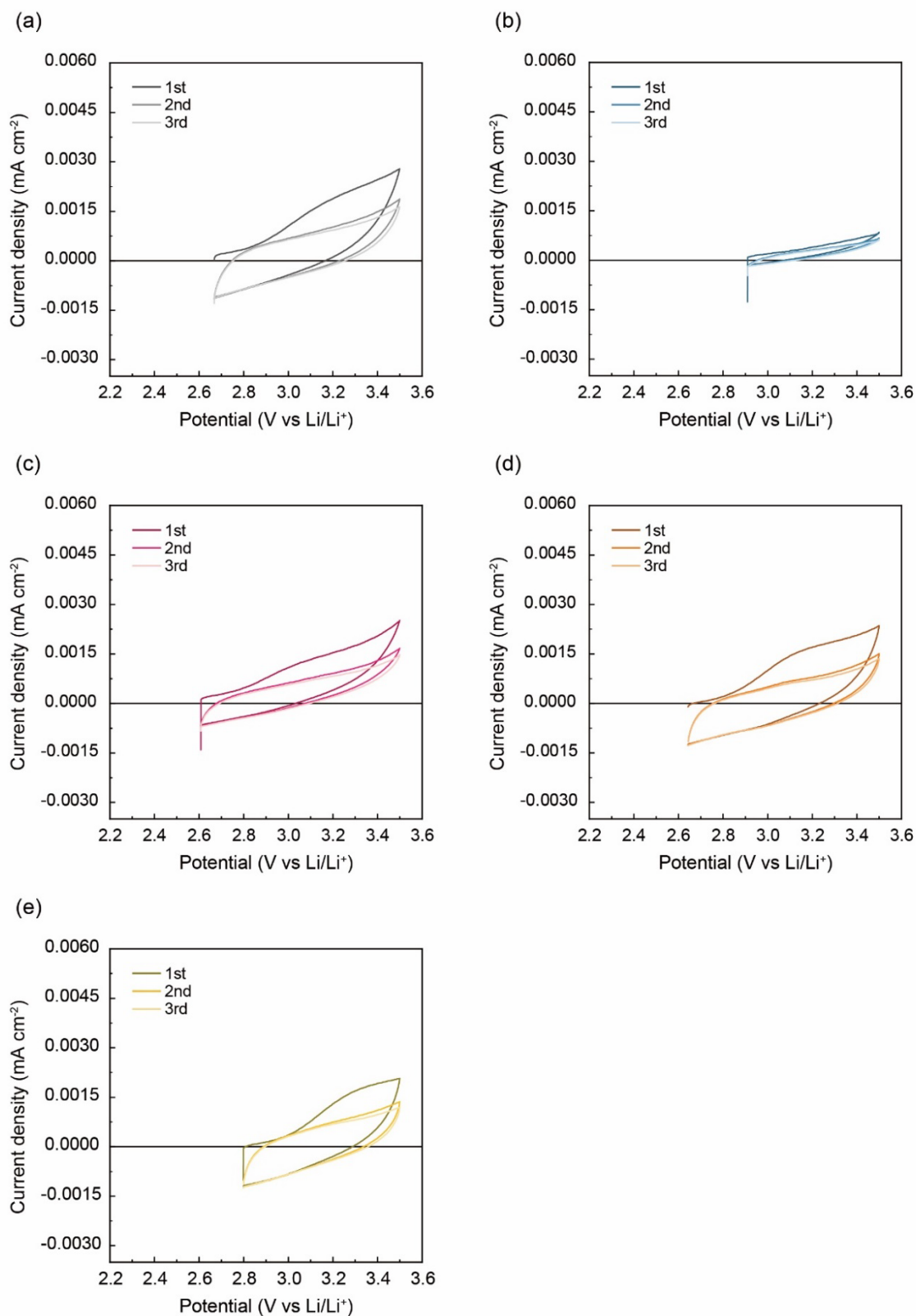


**Fig. S15** Cyclic voltammograms (CV) of Li||Al cells using (a) E1D1, (b) DBC, (c) BMEC, (d) B7E3, and (e) B1E1 electrolytes at a scan rate of 5 mV s<sup>-1</sup>. In order to eliminate the overpotential originated from Li metal anodes, the CV cycling was performed for 3 times in a voltage range from OCV to 3.5V before the LSV test shown in Fig. 2e.

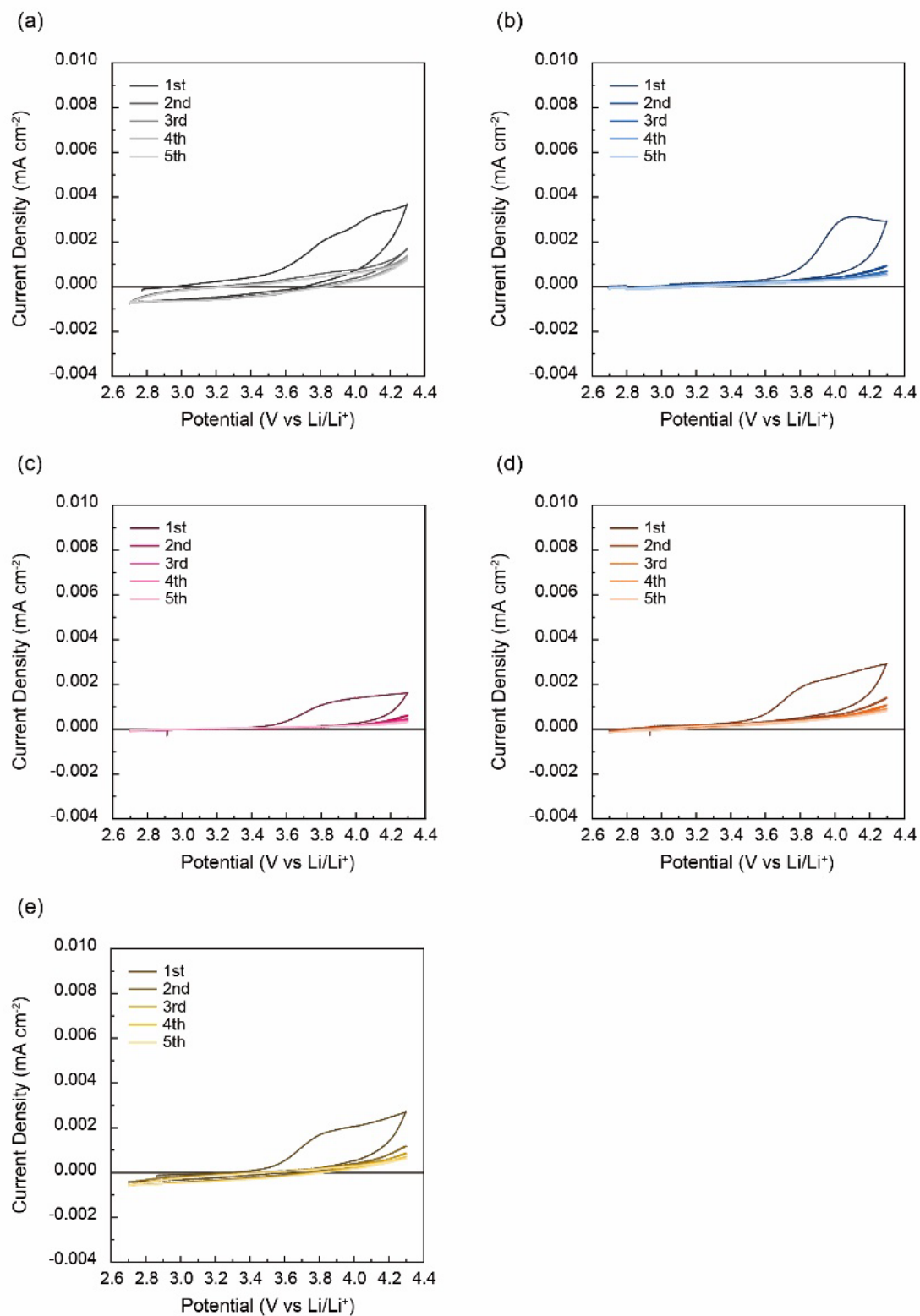


**Fig. S16** Cyclic voltammograms (CV) of Li||Al cells using (a) E1D1, (b) DBC, (c) BMEC, (d) B7E3, and (e) B1E1 electrolytes at a scan rate of 1 mV s<sup>-1</sup>. To clarify the oxidation stability of electrolytes in the conventional LIB operation window, the CV cycling was performed in a voltage range from 2.7 to 4.3 V.

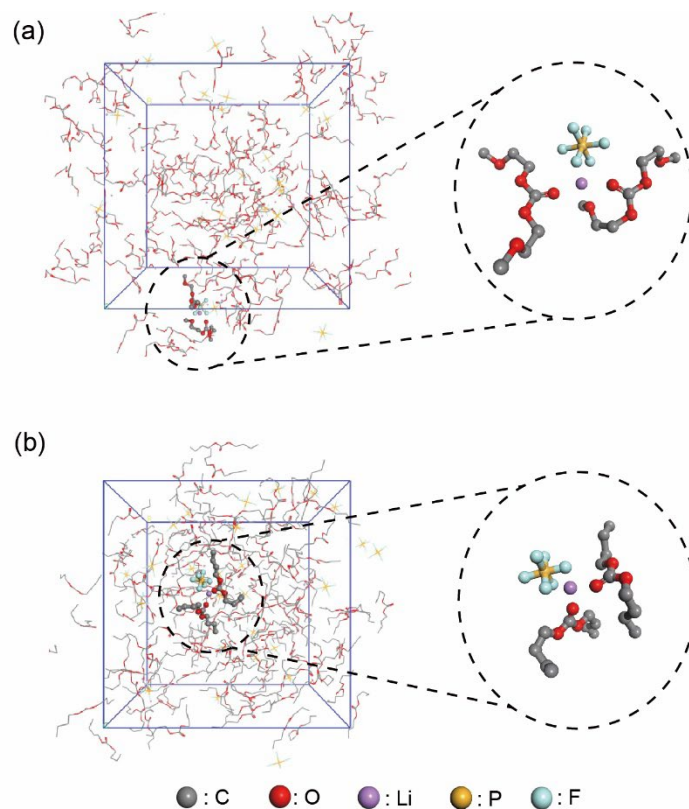


**Fig. S17** Li-ion solvation structures having PF<sub>6</sub><sup>-</sup> in the solvation shell from the simulation systems for (a) BMEC (BMEC 140 + LiPF<sub>6</sub> 23), and (b) DBC electrolytes (DBC 140 + LiPF<sub>6</sub> 27). In BMEC, a clamp-like Li ion solvation structure appears due to conformational changes even when PF<sub>6</sub><sup>-</sup> participate in solvation.

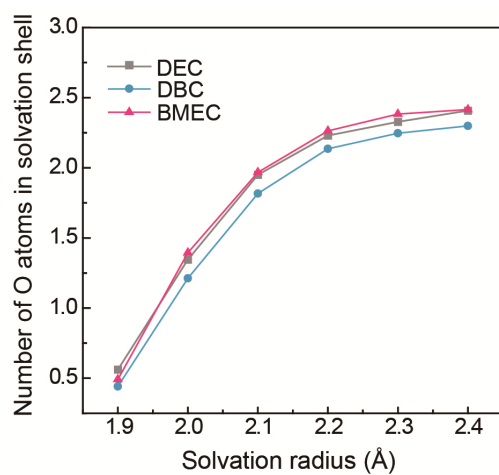


**Fig. S18** Number of O atoms in the solvation shell for each solvent by solvation radius. BMEC has more oxygen atoms participating in the solvation shell than DBC in a solvation radius range of 1.9–2.4 Å.

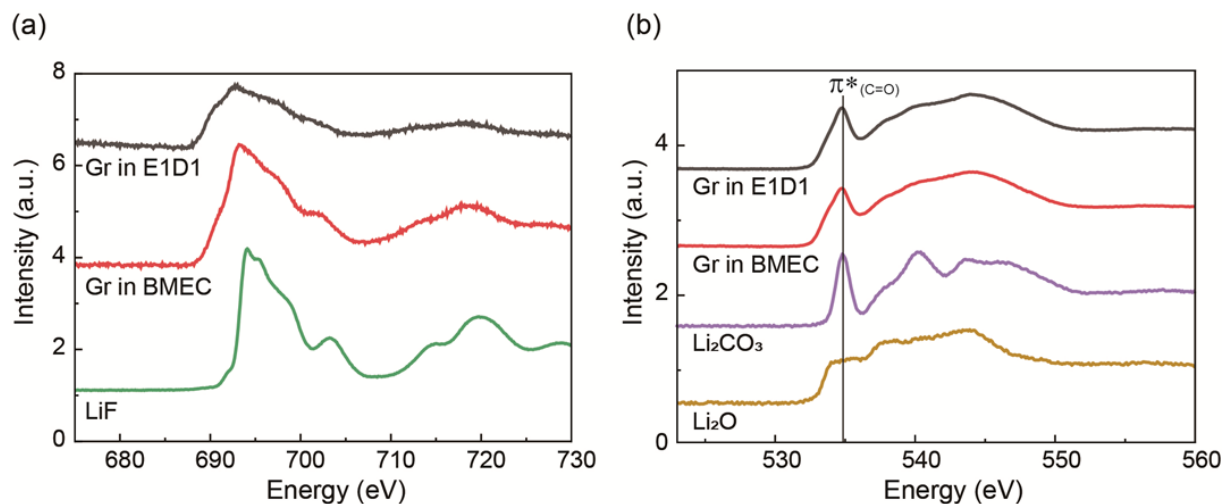


**Fig. S19** (a) F K-edge, (b) O K-edge NEXAFS spectra (TEY mode, ~10 nm depth) of graphite electrodes and reference chemicals (LiF, Li<sub>2</sub>CO<sub>3</sub>, and Li<sub>2</sub>O). The graphite electrodes were retrieved from Li||graphite cells that were discharged from OCV to 30 mV in E1D1 and BMEC electrolytes, respectively, at a current density of 0.2C (1C = 372 mAh g<sup>-1</sup>).

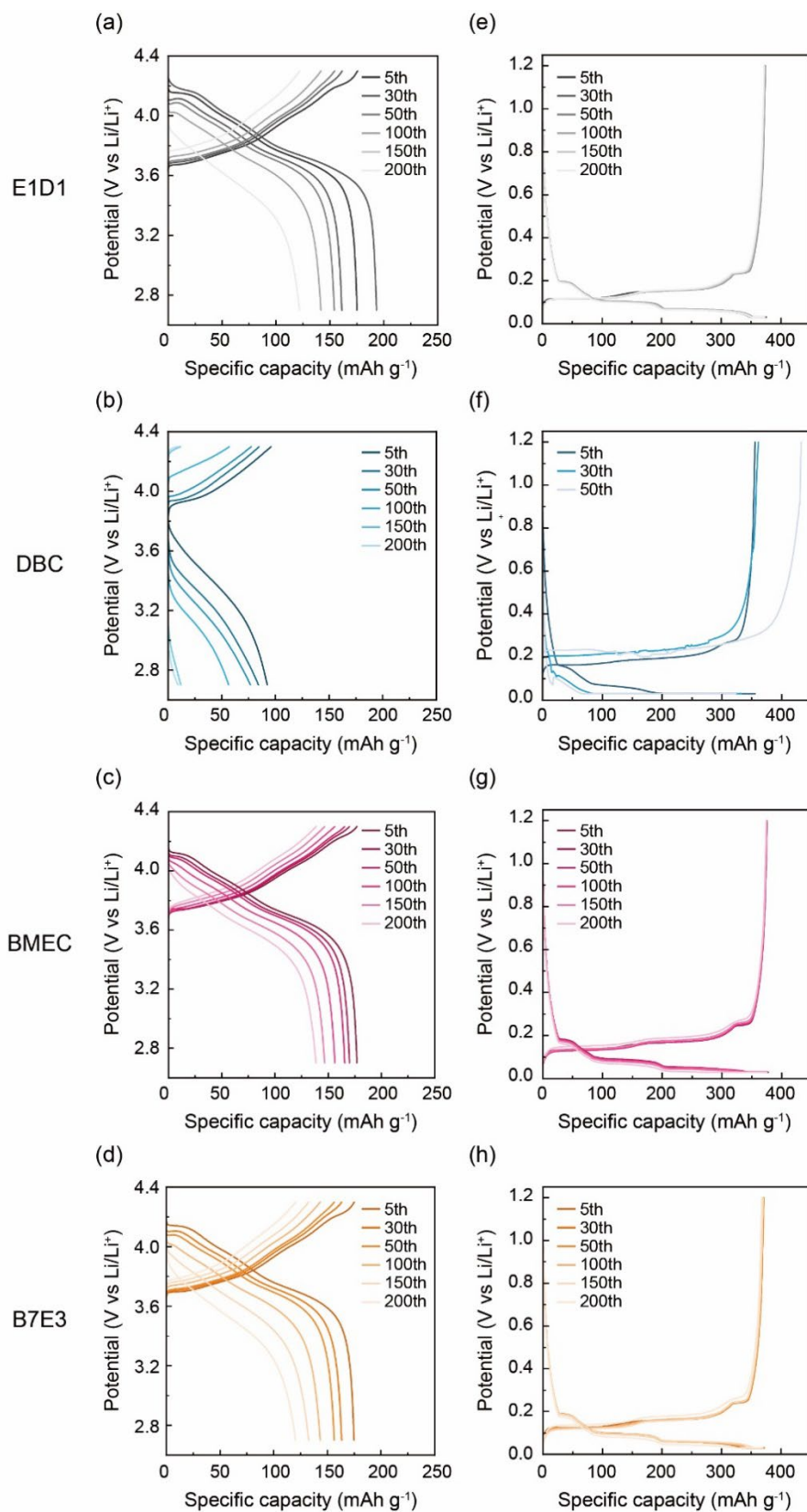


**Fig. S20** Voltage profiles of Li||NMC811 half cells using (a) E1D1, (b) DBC, (c) BMEC, and (d) B7E3 electrolytes at 0.5C (1C = 200 mAh g<sup>-1</sup>). Voltage profiles of Li||graphite half cells in (e) E1D1, (f) DBC, (g) BMEC, and (h) B7E3 electrolytes at 0.5C (1C = 372 mAh g<sup>-1</sup>).

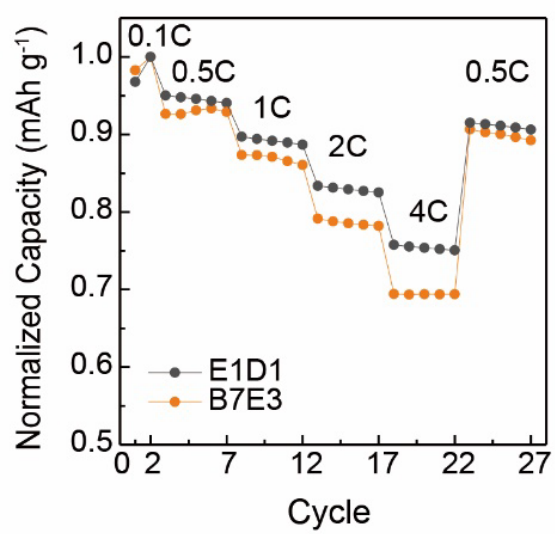


**Fig. S21** Performance of Li||NMC811 half cells in E1D1 and B7E3 at different C-rate from 0.1C to 4C (1C=200 mAh g<sup>-1</sup>). The capacity of half cells was normalized by second cycle at 0.1C.

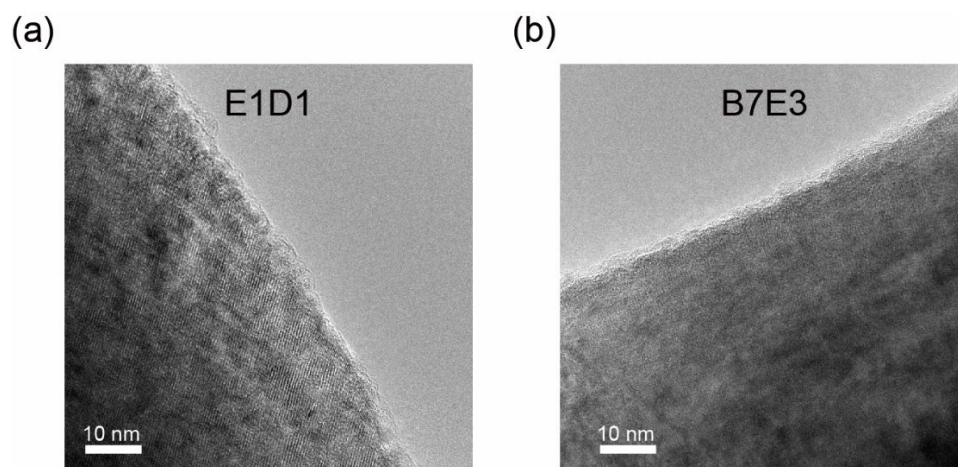


**Fig. S22** HR-TEM image of fully charged NMC811 cathode surface in (a) E1D1 and (b) B7E3. To observe the effect of electrolyte on cathode surface, the cathodes were cycled for three times at 0.1C and then fully charged to 4.3 V.

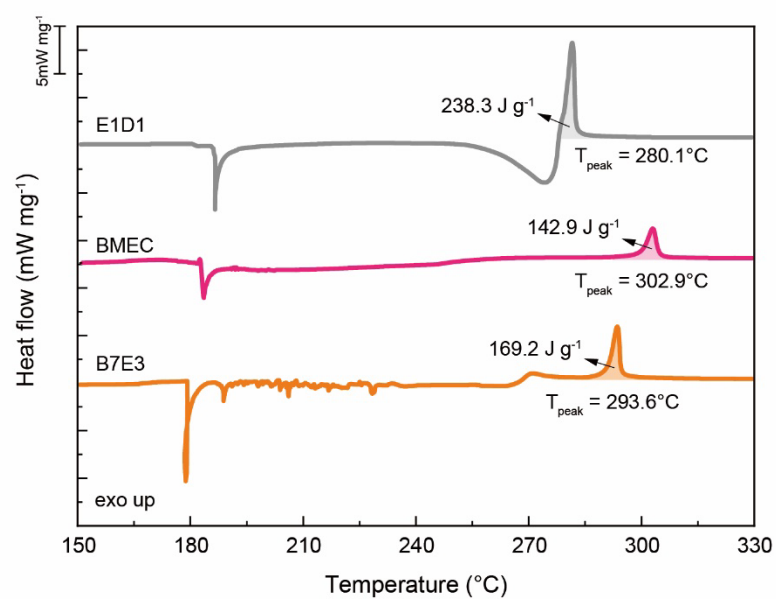


**Fig. S23** DSC curves of cycled NMC622 cathodes mixed with different electrolytes. The NMC622 powder was retrieved from Li||NMC622 half cells that were fully charged to 4.3 V after 3 formation cycles at 0.1C (1C = 180 mAh g<sup>-1</sup>).

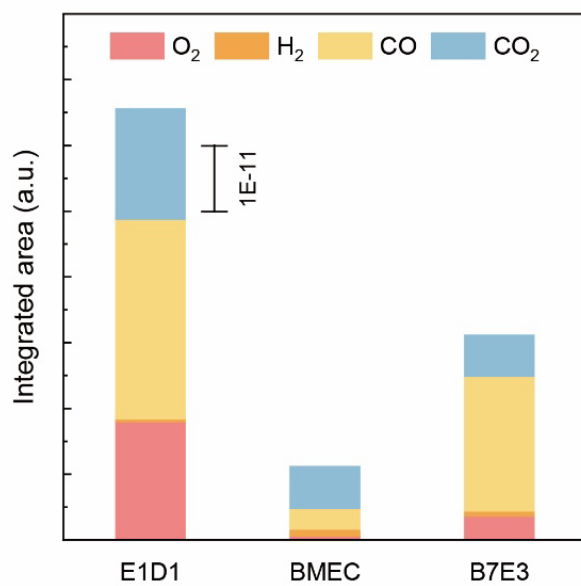


**Fig. S24** The integrated area of produced gas species upon heating only the electrolytes at 235°C, analyzed by a mass spectrometer.

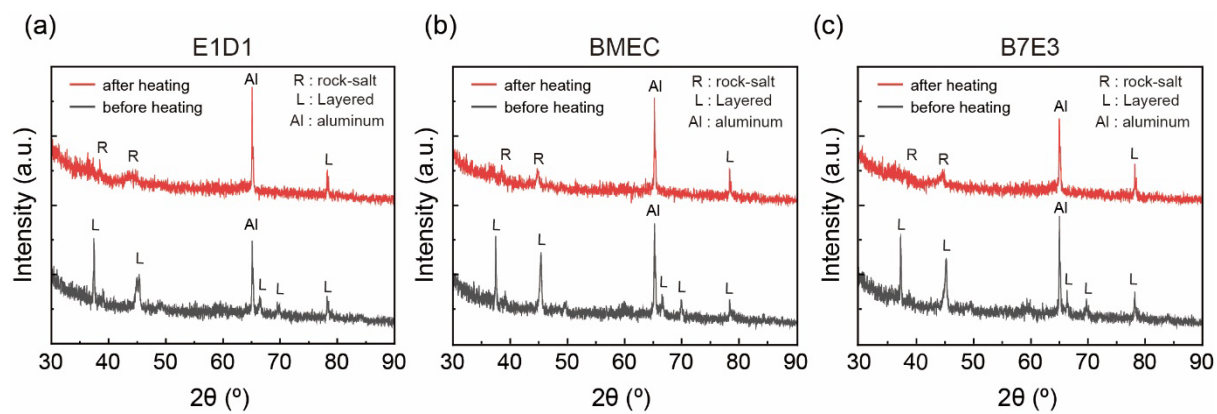


**Fig. S25** XRD profiles of fully charged NMC811 obtained from different electrolyte conditions and the corresponding sample after heating at 235°C. The cathodes were cycled using (a) E1D1, (b) BMEC, and (c) B7E3 electrolytes.

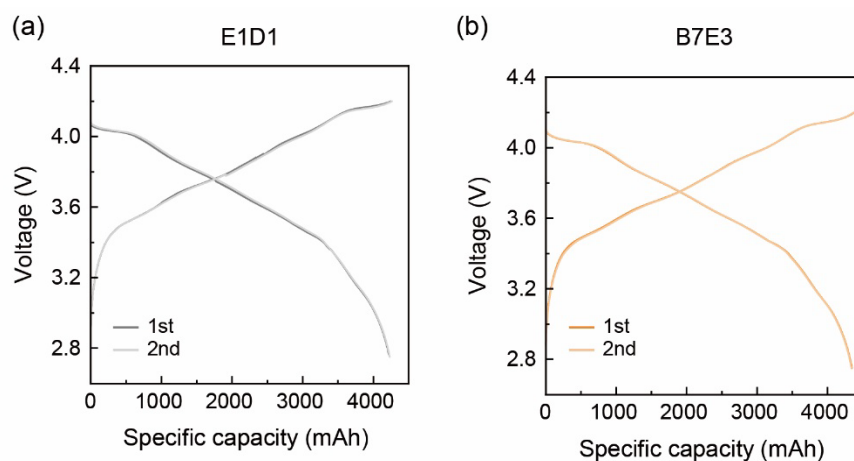


**Fig. S26** Voltage profiles of 4-Ah graphite||NMC811 pouch cells using (a) E1D1 and (b) B7E3 electrolyte. Each cell was cycled at 0.1C ( $1C = 4000 \text{ mAh g}^{-1}$ ) for two cycles in a voltage range of 2.75 to 4.2 V before being charged to 3.9 V for the nail-penetration test.

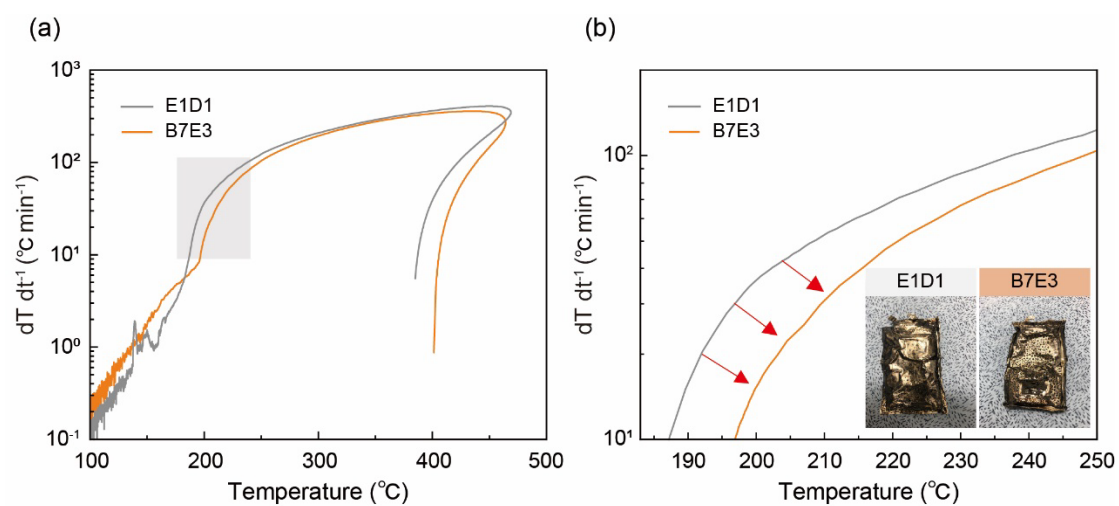


**Fig. S27** (a) ARC results of 1-Ah graphite||NMC811 batteries with E1D1 and B7E3. (b) The enlarged view of shaded area in (a) and photographs of pouch cells after the test.

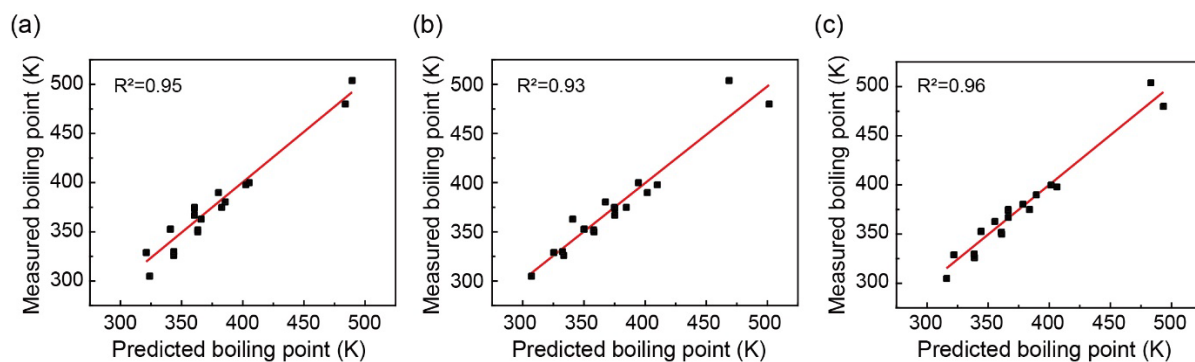


**Fig. S28** Performance of the linear regression models for predicting boiling point. The predicted boiling point values based on (a) molecular weight, (b) polarizability and (c) both molecular weight and polarizability (c) are plotted against the experimental boiling point values. The coefficients of determination ( $R^2$  score) are presented in each figure, indicating the accuracy of the model predictions.

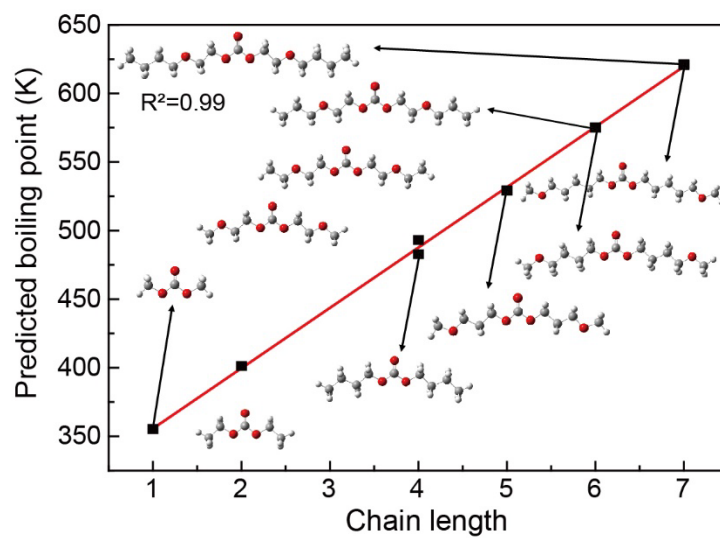
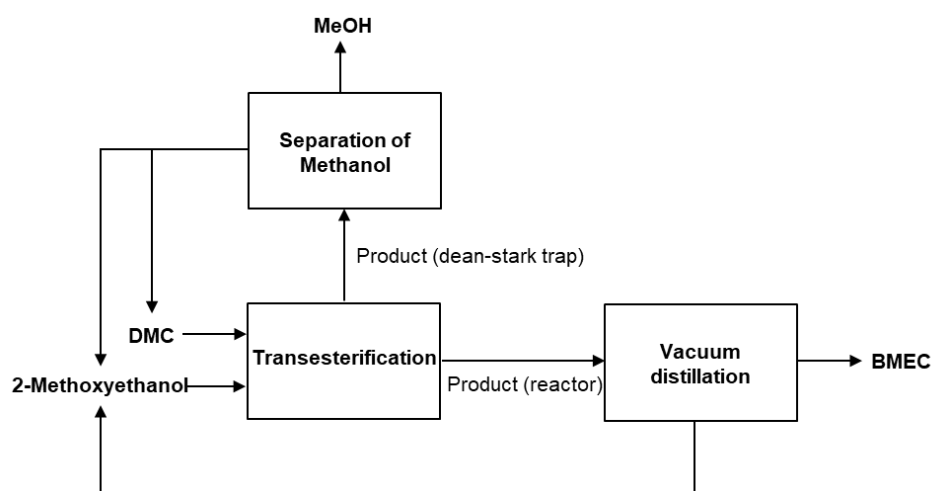


**Fig. S29** Predicted boiling points of symmetric carbonate solvents with increased symmetric alkyl chain lengths, based on the structure of BMEC. The graph includes the values of DEC and DBC, showing the boiling point trend with the chain length of linear carbonates.

**Scheme S1.** A diagram illustrating the proposed process of producing BMEC in a block flow format.



**Scheme S2.** Flowchart to simulate ionic conductivities of electrolytes.

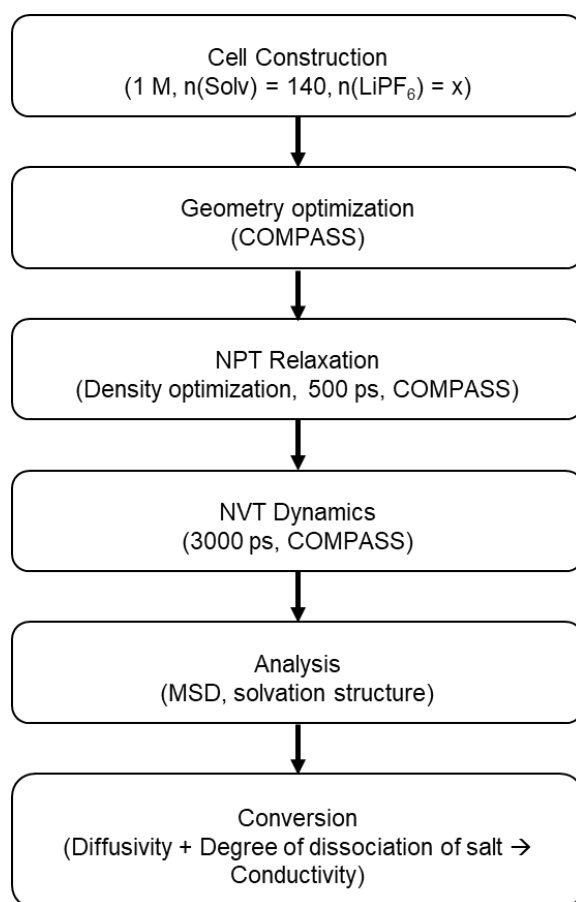
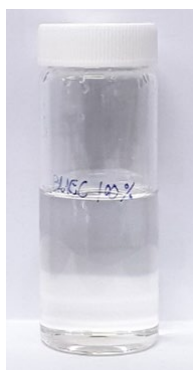


## Table S1-S7

**Table S1.** Purity evaluation of the isolated BMEC based on  $^1\text{H}$  qNMR spectra.

Compound	Integrals	Purity Evaluation
(+) Isolated BMEC: $M_{\text{BMEC}} = 178.18 \text{ g mol}^{-1}$ $W_{\text{BMEC}} = 5.9 \text{ mg}$	(+) Isolated BMEC: $I_{\text{BMEC}} = 1.25, N_{\text{BMEC}} = 4$ (proton signal of $\delta$ 4.29)	
(+) Standard: $M_{\text{std}} = 122.12 \text{ g mol}^{-1}$ $W_{\text{std}} = 5.3 \text{ mg}$ $P_{\text{std}} = 99.5\%$	(+) Standard: $I_{\text{std}} = 1, N_{\text{std}} = 2$ (proton signal of $\delta$ 8.13)	$P_{\text{BMEC}} \geq 99.9\%$



Purified BMEC

**Table S2.** Flash points of solvents.

Solvent	Flash point (°C)
EC	145
EC:DEC (1:1 vol%)	40
EC:BMEC (3:7 vol%)	127
EC:BMEC (1:1 vol%)	131

**Table S3.** Ionic conductivity values of electrolytes with GF/F separators at 30°C.

Electrolyte	log (S cm <sup>-1</sup> )	mS cm <sup>-1</sup>
DEC	-2.44	3.63
DBC	-3.67	0.21
D7E3	-3.29	0.51
E1D1	-2.12	7.59
BMEC	-2.84	1.45
B7E3	-2.52	3.02
B1E1	-2.39	4.07

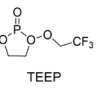
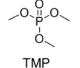
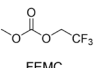
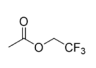
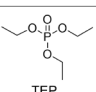
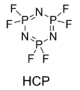
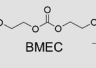
**Table S4.** Comparison of experimentally measured and calculated electrolyte densities (Temperature: 298 K).

COMPASS	BMEC-LiPF <sub>6</sub> (1 M)	DBC-LiPF <sub>6</sub> (1 M)	DEC-LiPF <sub>6</sub> (1 M)
1 <sup>st</sup>	1.171	0.965	1.074
2 <sup>nd</sup>	1.173	1.002	1.075
3 <sup>rd</sup>	1.17	1.005	1.07
Average	1.171	0.991	1.073
Exp. value	1.17	0.99	1.07
Error rate (%)	0.09	0.07	0.28

**Table S5.** HOMO and LUMO energy levels of solvents calculated by DFT.

Solvent	HOMO (eV)	LUMO (eV)
BMEC	-7.52	-0.30
DBC	-7.97	-0.27
DEC	-8.03	-0.24
DMC	-8.21	-0.24
EC	-8.47	-0.60
EMC	-8.14	-0.22

**Table S6.** Comparison of key properties and performances of nonflammable electrolyte.

Ref.	Electrolyte composition				F content (at %)	Molecular structure	Ionic conductivity (mS cm <sup>-1</sup> )	Electrolyte viscosity (cP)	Cell performance		
	x M	Salt	Solvent	Additive					Separator	Cell assembly	Cycling retention
(1)	0.95 M	LiFSI	TFEP:FEMC (1:3 vol %)	-	20		2.19	6.20	Glass fibre	Li    graphite	91.4% 400 cycle (C/2)
										Li    NMC111	80.1% 500 cycle (C/10)
(2)	5.3 M	LiFSI	TMP	-	-		2.2	72	Glass fibre	graphite    LiNMO	~93% 100 cycle (C/5)
	3.3 M	NaFSI	TMP	-	-						
(3)	1 M	LiPF <sub>6</sub>	EC:FEMC (3:7 vol %)	2 wt % VC	15.3		5.28	-	PP/PE/PP	graphite    NMC622	80% 100 cycle (C/2)
(4)	1 M	LiPF <sub>6</sub>	PC:TFA (3:7 vol %)	2 wt % FEC	15.2		7.09	3.4	PP/PE/PP	graphite    NMC622	89% 100 cycle (1C)
										graphite    NMC811 (pouch cell)	82% 400 cycle (1C)
(5)	0.05 M 2.8 M	LiBOB LiFSI	TEP	5 vol % FEC	0.19		1.3	-	Ceramic coated PE	graphite    LCO	90% 50 cycle (C/20)
(6)	0.8 M	LiPF <sub>6</sub>	EC:DEC:HCP (1:1.5:1 mol %)	-	12.2		5.23	6.21	PP/PE/PP	graphite    NMC622	~94% 200 cycle (C/2)
Our work	1 M	LiPF <sub>6</sub>	BMEC	-	0.11		1.45	13.02	PP/PE/PP	graphite    NMC811 (pouch cell)	91.4% 500 cycle (C/3)
			BMEC:EC (7:3 vol %)	3 vol % FEC	0.14		3.02	10.55			
			BMEC:EC (1:1 vol %)	-	0.17		4.07	9.95			

The full names of solvents present in the table are as follows: 2-(2,2,2-trifluoroethoxy)-1,3,2-dioxaphospholane 2-oxide (TFEP); 2,2,2-trifluoroethyl methyl carbonate (FEMC); Trimethyl phosphate (TMP); 2,2,2-trifluoroethyl acetate (TFA); Triethyl phosphate (TEP); Hexafluorocyclotriphosphazene (HCP).

The orange shaded area represents the demerits of the previous examples when adopted in practical LIBs. While dramatically improving thermal safety, molecular engineering of linear carbonate (BMEC-based electrolytes) demonstrated in this study does not compromise the essential properties as a practical electrolyte such as ionic conductivity, viscosity, synthetic cost, inherent toxicity (mainly from intensive halide usage), compatibility with commercial cell components, and adaptability to commercial manufacturing processes.

The F atomic content in each electrolyte was calculated by using the following equation,

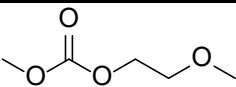
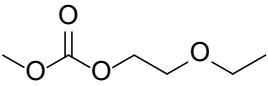
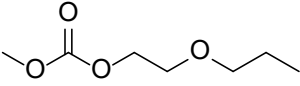
$$\text{F content (at \%)} = \frac{\text{mole of F in mixture}_{\text{solvent+additive}}}{\text{mole of total atoms}_{\text{solvent}} + \text{mole of total atoms}_{\text{additive}}}$$

#### Reference list of the nonflammable electrolyte examples in Table S6

1. Zheng, Q., Yamada, Y., Shang, R., Ko, S., Lee, Y.-Y., Kim, K., Nakamura, E., and Yamada, A., *Nat. Energy*, 2020, **5**, 291-298.
2. Wang, J., Yamada, Y., Sodeyama, K., Watanabe, E., Takada, K., Tateyama, Y., and Yamada, A., *Nat. Energy*, 2018, **3**, 22-29.
3. Chung, G.J., Han, J., and Song, S.W., *ACS Appl. Mater. Interfaces*, 2020, **12**, 42868-42879.
4. An, K., Tran, Y.H.T., Kwak, S., Han, J., and Song, S.W., *Adv. Funct. Mater.*, 2021, **31**, 2106102.

5. Zeng, Z., Murugesan, V., Han, K.S., Jiang, X., Cao, Y., Xiao, L., Ai, X., Yang, H., Zhang, J.-G., Sushko, M.L., and Liu, J., *Nat. Energy*, 2018, **3**, 674-681.
6. Tan, S.-J., Tian, Y.-F., Zhao, Y., Feng, X.-X., Zhang, J., Zhang, C.-H., Fan, M., Guo, J.-C., Yin, Y.-X., Wang, F., et al., *J. Am. Chem. Soc.*, 2022, **144**, 18240-18245.

**Table S7.** Predicted boiling points of asymmetric carbonates using a trained model.

Molecular Structure	Polarizability ( $\text{\AA}^3$ )	Molecular Weight ( $\text{g mol}^{-1}$ )	Predicted Boiling point (K)
 (2-methoxyethyl) methyl carbonate (MEMC)	77.15	134.13	405.8
 (2-ethoxyethyl) methyl carbonate (EEMC)	89.99	148.16	425.9
 Methyl 2-propoxy ethyl carbonate (MPEC)	102.46	162.18	447.2

## Note S1

### **Note S1.** general applicability of our alkyl chain extension and alkoxy substitution strategy

We believe that this strategy can be applied to other linear organic carbonates to reduce solvent volatility. As volatility is typically evaluated through measurements of vapour pressure or boiling point, we focused on boiling point as a proxy for volatility in our predictions. To investigate the applicability of our strategy to other linear organic carbonates, we first build the regression model to predict boiling points using experimental values of 20 solvent molecules with carbonyl groups. In the literature, different descriptors have been proposed for predicting boiling points.<sup>11</sup> In this study, we chose to focus on two factors, molecular weight and polarizability, which have shown high Pearson correlation coefficients, 0.965 and 0.972, respectively, with boiling points for our dataset of 20 solvent molecules. In this case, the polarizability was calculated using Gaussian 16. We trained linear regression models for predicting boiling point using molecular weight, polarizability, and both variables simultaneously as predictors, as shown in **Fig. S28**. The  $R^2$  score indicates the goodness of fit between the predicted values and experimental values; thus, a higher  $R^2$  indicates a better fit. As shown in **Fig. S28**, the model using both molecular weight and polarizability as predictors has the highest  $R^2$  score of 0.96, indicating the most accurate prediction of boiling point among the three models.

Using our trained model, we predicted the boiling points of other carbonate molecules having asymmetric alkoxyalkyl substitutions, such as (2-methoxyethyl) methyl carbonate (MEMC), 2-ethoxyethyl methyl carbonate (EEMC), and methyl 2-propoxy ethyl carbonate (MPEC). The molecular structure, polarizability, molecular weight, and predicted boiling point values for the three molecules are presented in **Table S7**. These molecules share a similar core structure, while the chain length of alkoxyalkyl increases in the order of MEMC<EEMC<MPEC. The results show that the boiling points of asymmetric carbonate solvents increase with chain length as both polarizability and molecular weight increase with chain length.

We also predicted the boiling points of symmetric carbonate solvents, of which the alkyl chain length increased symmetrically, using the structure of BMEC as a basis. We generated hypothetical molecular structures by extending the chain length in two distinct ways: either by increasing the alkyl chain length between the carbonate structure and the ether oxygen or by expanding the alkyl chain length outside the ether oxygen. In this context, "chain length" refers to the length of one chain relative to the carbonate structure, encompassing both oxygen and carbon elements. **Fig. S29** illustrates the predicted boiling points in relation to chain lengths, indicating that the boiling points rise with the increasing chain length of linear carbonates.

Our findings suggest that for both asymmetric and symmetric carbonates with similar basic skeletons, the boiling point rises as the chain length increases. Consequently, we expect volatility to decrease with increasing chain length. Nevertheless, further research is necessary to understand the conductivity aspect, as viscosity and solvation ability are also anticipated to change with chain lengths.

## References

1. James Evans, C.A.V., Peter G.Bruce, *Polymer*, 1987, **28**, 2324-2328.
2. Sun, H., *J. Phys. Chem. B*, 1998, **102**, 7338-7364.
3. Akkermans, R.L.C., Spenley, N.A., and Robertson, S.H., *Mol. Simul.*, 2021, **47**, 540-551.
4. Lee, C., Yang, W., and Parr, R.G., *Phys. Rev. B*, 1988, **37**, 785-789.
5. Frisch, M.J., Trucks, G.W., Schlegel, H.B., Scuseria, G.E., Robb, M.A., Cheeseman, J.R., Scalmani, G., Barone, V., Petersson, G.A., Nakatsuji, H., et al., *Gaussian*, 2016, **16** Rev. C.01.
6. Ong, S. P., Richards, W. D., Jain, A., Hautier, G., Kocher, M., Cholia, S., ... & Ceder, G., *Comput. Mater. Sci.*, 2013, **68**, 314-319.
7. Kameda, Y., Saito, S., Umebayashi, Y., Fujii, K., Amo, Y., & Usuki, T., *J. Mol. Liq.*, 2016, **217**, 17-22.
8. Pedregosa, F., Varoquaux, G., Gramfort, A., Michel, V., Thirion, B., Grisel, O., ... & Duchesnay, E., 2011, **12**, 2825-2830.
9. Ehresmann, B., de Groot, M. J., Alex, A., & Clark, T, *J. Chem. Inf. Comput. Sci.* 2004, **44**, 658–668.
10. Schoenberger, T. (2012). *Anal. Bioanal. Chem.*, 2012, **403**, 247-254.
11. Ehresmann, B., de Groot, M. J., Alex, A., & Clark, T. (2004). *J. Chem. Inf. Comput. Sci.*, **44**, 658-668.